The Effects of Desiccation and Climatic Change on the Hydrology of the Aral Sea

ERIC E. SMALL

Department of Earth and Environmental Science, New Mexico Institute of Mining and Technology, Socorro, New Mexico

FILIPPO GIORGI

Physics of Climate Group, Abdus Salam International Center for Theoretical Physics, Trieste, Italy

LISA CIRBUS SLOAN

Department of Earth Science, University of California, Santa Cruz, Santa Cruz, California

STEVEN HOSTETLER

U.S. Geological Survey, Corvallis, Oregon

(Manuscript received 17 September 1999, in final form 10 February 2000)

ABSTRACT

Anthropogenic desiccation of the Aral Sea between 1960 and the mid-1990s resulted in a substantial modification of the land surface that changed air temperature in the surrounding region. During the desiccation interval, the net annual rate of precipitation minus evaporation ($P - E$) over the Aral Sea's surface became more negative by ~15%, with the greatest changes occurring during the summer months. In addition, Aral Sea surface temperatures (SST) increased by up to 5°C in the spring and summer and decreased by up to 4°C in the fall and winter. A series of coupled regional climate–lake model experiments were completed to evaluate if the observed hydrologic changes are caused by desiccation or instead reflect larger-scale climatic variability or change, or some combination of both. If the $P - E$ changes are the result of desiccation, then a positive feedback exists that has amplified the anthropogenic perturbation to the hydrologic system.

The effects of desiccation are examined by varying the simulated area, depth, and salinity of the Aral Sea in different model experiments. The simulated changes in SST resulting from desiccation are similar to the observed changes—both simulated and observed SSTs have increased during the spring and summer and have decreased during the fall and winter. The simulated changes in the annual cycle of $P - E$ resulting from desiccation are also similar to observed changes, but the simulated net annual decrease in $P - E$ is only ~30% of the observed decrease. Warming has been observed across central Asia during the desiccation interval. The hydrologic response to this large-scale climatic variability or change was assessed by perturbing the meteorological boundary conditions (1.5°C cooling with constant relative humidity) but leaving the Aral Sea characteristics unchanged. The simulated effects of warming do not closely match the observed changes on the monthly timescale—SST changes are positive and the $P - E$ changes are negative in all months. However, the annual change in $P - E$ is similar to the observed value.

The simulated hydrologic response to the combined effects of desiccation and warming matches the observed SST and $P - E$ changes more closely than the response to each forcing alone. This result indicates that a combination of both desiccation and climatic change or variability has produced the observed hydrological changes—the primary effect of desiccation is to alter the annual cycle of SST and $P - E$ whereas warming has modified the hydrologic budget on the annual timescale.

1. Introduction

The surface area of the Aral Sea was ~65 000 km^2 in 1960, making it the fourth largest inland water body on Earth (Fig. 1). The Aral Sea is a terminal lake (no outflow) and receives inflow only from the Amu and Syr Darya Rivers. After 1960, agricultural diversions of river water increased substantially throughout the Aral Sea drainage basin (Micklin 1988). The river inflow to the Aral was greatly reduced because most of the diverted water was lost to evapotranspiration and groundwater recharge. As a result of the reduced inflow, the water balance of the Aral Sea became negative after 1960—evaporation from the lake surface was greater than the sum of on-lake precipitation and the reduced

Corresponding author address: Dr. Eric Small, Dept. of Earth and Environmental Science, New Mexico Tech, Socorro, NM 87801.
E-mail: esmall@nmt.edu

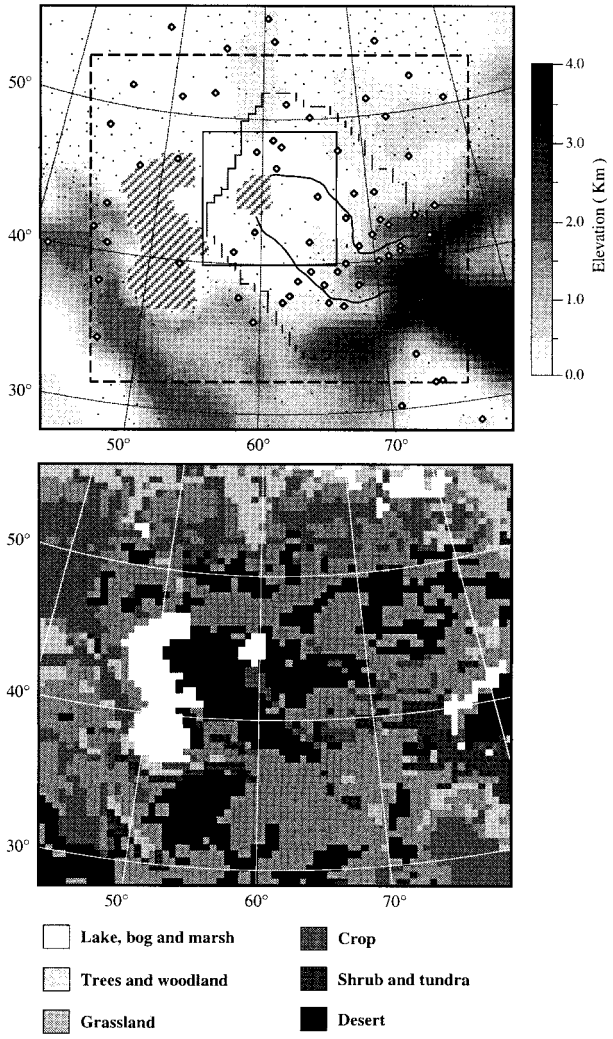

FIG. 1. Numbers on outside of maps indicate °N and °E (top). Shading depicts surface elevation. The Caspian (left) and Aral Seas (center) are hatched. The irregularly shaped polygon shows the Aral Sea drainage basin boundary and the two curves ending at the Aral Sea represent the Amu Darya (south) and Syr Darya (north). The dashed rectangle shows the inner edge of the buffer zone throughout which boundary conditions are applied. (bottom) Biosphere–Atmosphere Transfer Scheme (BATS) land cover categories for the model domain. Similar categories (e.g., tall and short grass) have been shaded similarly.

streamflow. The result was 1) an ~60% decrease in lake surface area, 2) a decrease in mean depth from 15 to 8 m, 3) an 80% decrease in volume, and 4) an increase in salinity from 10 to >35 ppt (Table 1). The magnitude of these changes increased throughout the 1990s.

Desiccation of the Aral Sea, therefore, has resulted in a substantial and spatially extensive modification of the land surface. By 1998, ~40 000 km^2 that was once part of the lake had been replaced by sparsely vegetated sand and evaporite deposits, leading to important changes in the thermal, moisture, and radiative properties of the land surface. The ~25 000 km^2 of the Aral Sea remaining in 1998 had also been affected. The thermal capacity of the extant portions of the lake decreased due to the reduction in depth, which has modified the temperature of the lake surface and the evaporation rate.

TABLE 1. Observed Aral Sea surface area, average depth, volume, and salinity in 1960 and 1990. The corresponding values used in the Full Lake and Half Lake experiments are also shown, as well as the number of 50 km × 50 km grid cells covered by the Aral Sea.

	Observed 1960	Model (Full Lake)	Observed 1990	Model (Half Lake)
Surface area (10^3 km^2)	65–75	70	37	35
Number of model grid cells		28		14
Average depth (m)	15	16	8	10
Volume (km^3)	1100	1150	300	350
Salinity (ppt)	10	10	33	33

Changes in land–atmosphere interactions from desiccation have resulted in dramatic surface air temperature changes in the Aral Sea region. Small et al. (2001, this issue) identified the climatic changes resulting from desiccation by isolating temperature trends unique to the Aral Sea region. The climate records from around the Aral Sea show dramatic temperature changes between 1960 and 1997, once regionally coherent trends and variability are removed. Mean, maximum, and minimum temperature near the Aral Sea have changed by up to 8°C. Warming (cooling) is observed during spring and summer (fall and winter), as expected to accompany the diminished ''lake effect'' caused by desiccation. The magnitude of changes decreases with distance from the 1960 shoreline, with changes extending up to ~200 km from the shoreline in the downwind direction. An increase in diurnal temperature range (DTR) of 2°–3°C is observed in all months, demonstrating a weakening of the lake's damping effect on the diurnal temperature cycle.

Accompanying these local changes in air temperature, substantial hydrologic changes have occurred between 1960 and the mid-1990s, which are described for the first time in this paper (section 2). The net annual rate of precipitation minus evaporation ($P - E$) over the lake's surface has become more negative, with the greatest change occurring during the summer months. This change has enhanced the reduction in the volume of the Aral Sea by 15% over that due to changes in river inflow. In addition, Aral Sea surface temperatures (SSTs) have increased in the spring and summer and decreased in autumn and winter. These changes are closely tied to the changes in $P - E$, as the lake surface temperature influences both evaporation and on-lake precipitation.

The purpose of this paper is to identify the processes responsible for the observed hydrologic changes ($P - E$ and SST) that have accompanied desiccation. We compare the effects of desiccation, large-scale climatic variability or change, and the combination of these two forcings. If the $P - E$ changes are the result of desiccation, then a positive feedback exists that has amplified

the anthropogenic perturbation to the Aral Sea hydrologic system. However, if the observed changes in $P - E$ and SST are the result of large-scale warming, then there is no evidence to support the existence of a lake size–water balance feedback. Instead, large-scale climatic change or variability has enhanced the effects of the anthropogenic reduction in river discharge.

It is not possible to use observations alone to identify the component of the observed hydrologic changes that has resulted from desiccation, as was done for changes in air temperature (Small et al. 2001). Water bodies similar to the Aral Sea do not exist throughout central Asia. Consequently, there are no ''control'' lakes that have not experienced desiccation that can be used to identify regionally coherent hydrologic trends caused by large-scale climatic variability or change. Therefore, we use a modeling approach to compare the effects of desiccation and large-scale climatic variability or change on the hydrology of the Aral Sea. We have completed several continuous, 5-yr simulations using the National Center for Atmospheric Research's (NCAR) regional climate model (RegCM2) interactively linked to a lake model. The performance of this coupled modeling system in simulating the present-day climate and hydrologic behavior of the Aral Sea is described elsewhere (Small et al. 1999a,b).

In order to identify the causes of the hydrologic changes that have accompanied desiccation, we first examine two related questions: 1) How does the Aral Sea affect regional climate? 2) Given the climatic influence of the Aral, are the observed changes in $P - E$ and SST likely to be caused by desiccation since 1960? Previous observational (e.g., Changnon and Jones 1972) and modeling studies (e.g., Bates et al. 1995) have shown that each of the U.S. Great Lakes individually exerts a strong influence on the climate of the surrounding region, primarily driven by the seasonally varying water-to-land temperature contrast (Miner and Fritsch 1997). This effect on regional climate influences the water balance of the lakes by changing the rates of evaporation and precipitation both over the lakes and throughout their hydrologic basins. For example, it has been estimated that wintertime precipitation is enhanced by 30%–50% in the area downwind of each of the Great Lakes (Eichenlaub 1970). Using a modeling approach similar to that applied here, Hostetler et al. (1994) found that paleolake Bonneville enhanced precipitation within its drainage basin, representing a positive feedback on the lake's hydrologic budget. The Aral Sea influences the climate in the surrounding region (Small et al. 2001) and is similar in size to the largest Great Lakes and to paleolake Bonneville. Therefore, it is reasonable to expect that the Aral Sea affects its own hydrology, allowing for feedbacks between desiccation and the hydrologic state of the sea.

We also examine whether the observed $P - E$ and SST changes were caused by large-scale climatic change or variability between 1960 and the 1990s. Over the interval of desiccation, air temperatures have increased throughout the Northern Hemisphere (Houghton et al. 1996). This warming is evident throughout central Asia, where temperatures have increased by up to 1.5°C (Fig. 2), and should influence the hydrology of the Aral Sea. Some component of the observed warming may be due to enhanced greenhouse gas concentrations (Houghton et al. 1996). In the cold season, a substantial component of the warming is due to a trend in the state of the ocean–atmosphere system, as indicated by the North Atlantic oscillation index (NAO) (Hurrell and van Loon 1997). Since 1960, the NAO has slowly drifted from very negative to very positive values, which represents an increase in the strength of zonal flow and advection of warm air from the North Atlantic into central Asia.

The plan of this paper is as follows. First, we describe the observed $P - E$ and SST changes that have accompanied desiccation of the Aral Sea (section 2). Then we describe the coupled RegCM2-lake model and the experiments used to study the observed changes in $P - E$ and SST (section 3). We then assess the simulated climatic effects of the Aral Sea (section 4) and how desiccation influences the lake's hydrologic processes (section 5). Next, we examine how climatic change or variability over the past 40 years influences the simulated water balance of the Aral Sea (section 6). A summary concludes the paper (section 7).

2. Observed hydrologic changes

a. Aral Sea water balance ($P - E$)

The rate of change in volume of the Aral Sea (dV/dt) represents the balance between the volume of streamflow entering the lake (S) and the rates of precipitation (P) and evaporation (E) over the lake's surface area (A_L):

$$\frac{dV}{dt} = S + A_L(P - E). \tag{1}$$

The groundwater contribution to the Aral Sea's hydrologic budget is estimated to be minor (Sadov and Krasnikov 1987), so we assume it is zero. Direct measurements of precipitation (P) and evaporation (E) over the Aral Sea do not exist. Therefore, we calculate the combined contribution of precipitation and evaporation averaged over the lake, $P - E$, as a residual in the above water balance equation.

$$(P - E) = \frac{\dfrac{dV}{dt} - S}{A_L} = \Delta SL - \frac{S}{A_L}. \tag{2}$$

Monthly values of $P - E$ averaged over the Aral Sea are determined from a monthly time series of sea level (SL), streamflow entering the lake from the Amu and Syr Darya, and surface area observations, for the period 1950–93. Annual data are used to calculate net annual $P - E$ beginning in 1926.

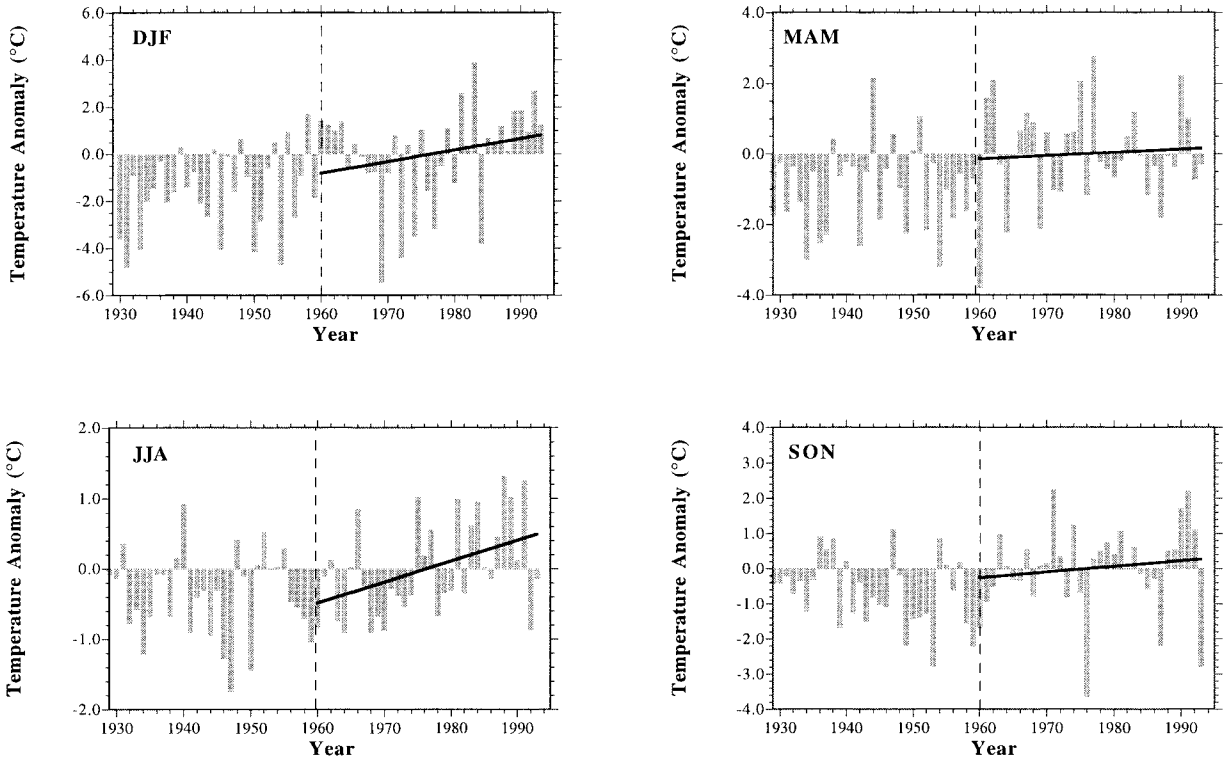

FIG. 2. Seasonal temperature anomalies averaged over the region 40°–55°N and 45°–75°E, from the Jones 5° × 5° global temperature dataset. Only two of the ~100 stations in the analyzed region are within several hundred kilometers of the Aral Sea. Therefore, the observed temperature changes do not reflect Aral Sea desiccation but instead reflect large-scale climatic variability or change. DJF is Dec–Feb, MAM is Mar–Apr, JJA is Jun–Aug, and SON is Sep–Nov. Anomalies are calculated from the 1960–93 mean for each season. The solid lines are least squares fit for the interval 1960–93. The onset of desiccation (1960) is shown (dashed lines). The temperature scale is different for each season.

The annual rate of $P - E$ decreased substantially after 1960 (Fig. 3a). Nearly half of the post-1960 values are lower than the pre-1960 minimum. (The outlier in 1991 is excluded from all calculations.) Linear regression indicates the change since 1960 is -122 ± 45 mm yr^{-1} (95% confidence interval estimate) or 13%. However, the change is only approximately linear. Over the last 10 yr of the record, the average rate is -992 mm yr^{-1}, a decrease of 163 mm yr^{-1} or 17% in comparison with the pre-1960 mean (-829 mm yr^{-1}). Neither linear regression or comparing the final 10 yr of the record to pre-1960 value is perfect. Therefore, we use the midpoint of the values, -141 mm yr^{-1} or 15%, as an estimate of the annual change in $P - E$ that has accompanied desiccation of the Aral Sea. We estimated monthly changes in $P - E$ by completing linear regressions independently for each month of the year. The greatest change is in August (-50 mm; Fig. 3b), which is the month when $P - E$ is most negative (Small et al. 1999b; Fig. 12). Precipitation minus evaporation becomes more negative between May and September and less negative in October and November. The contributions of precipitation and evaporation changes to the observed $P - E$ changes are discussed in section 4.

These $P - E$ changes are rough estimates because the streamflow values used in the water balance calculation may not accurately represent the amount of water added to the Aral Sea. The gauging stations on the Amu Darya and Syr Darya rivers are ~50–100 km upstream of the Aral Sea shore. Instead of reaching the lake, some fraction of the water passing the gauge site may evaporate from wetlands or infiltrate to groundwater. In the above calculations, we assumed that all gauged streamflow reaches the Aral Sea, which yields a minimum $P - E$ estimate for each month. In many months, the minimum estimate nearly matches the actual value because flow in the Amu and Syr Darya is often negligible. The water loss between gauges and the lake has decreased through time, in terms of percent and total volume of flow, as the streams have become entrenched below the level of the deltas (P. P. Micklin 1998, personal communication). If we included this transient increase of streamflow into the lake in our calculations, $P - E$ would become even more negative between 1960 and the mid-1990s. Therefore, the changes presented here should be viewed as minimum estimates of the actual $P - E$ changes.

Temporary storage of runoff in wetlands or near-surface aquifers between the gauging stations and the Aral Sea result in $P - E$ errors for a particular month. If the

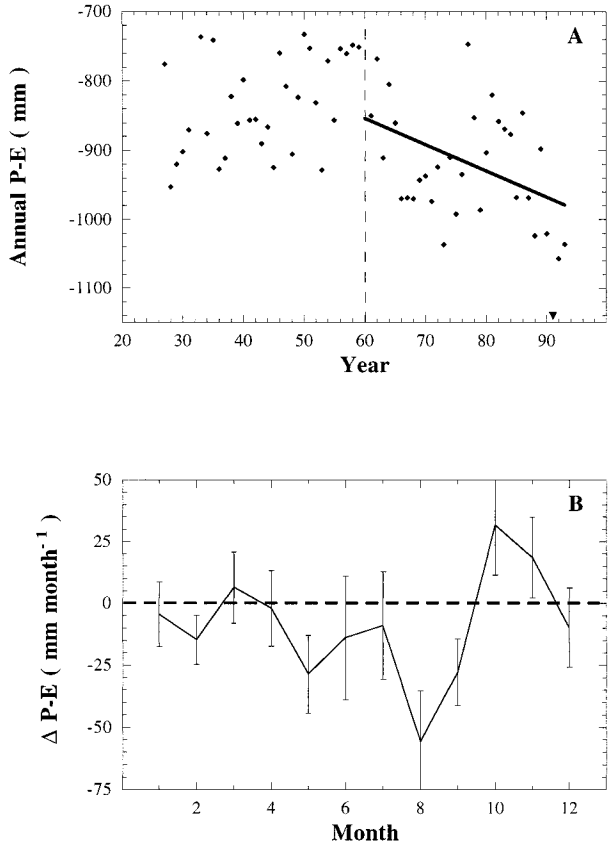

FIG. 3. (a) Annual values of $P - E$ over the Aral Sea, from 1926 through 1992. All values are negative because evaporation exceeds precipitation. The dashed line indicates the onset of desiccation. The solid line is a linear fit to the observations between 1960 and 1993. The value from 1991 is plotted (triangle) but is not included in the regression. (b) Changes in $P - E$ over the Aral Sea by month. The error bars represent the 95% confidence interval estimate on the change, based on the linear regression for each month.

magnitude and duration of temporary storage has changed since 1960, this would influence the relative magnitude of observed $P - E$ changes in different months (Fig. 3b). Therefore, it is possible that the large change in August actually represents a substantial change throughout the summer.

b. Aral Sea surface temperature

We use two datasets to examine changes in Aral Sea surface temperature: 1) in situ SST data acquired from the State Oceanographic Institute in Russia, and 2) Multi-Channel Sea Surface Temperature (MCSST) data derived from the NOAA Advanced Very High Resolution Radiometer (AVHRR) (McClain 1989; McClain et al. 1985). The in situ SST data were measured during ~100 boat surveys between 1960 and 1992. The frequency of surveys decreased substantially after 1980. SST was measured at a depth of 0.5 m. The satellite data are available starting in 1984. AVHRR measurements are converted to SSTs based on a set of calibration coefficients determined from a previous comparison between AVHRR data and buoy-derived SSTs. Compared to simultaneous buoy and boat measurements from around the world that were not included in the calibration, instantaneous MCSST observations exhibit a mean cold bias of ~0.35°C with a standard deviation of 0.65°C (McClain, 1989). The version of the data used here has a spatial resolution of ~17 km and consists of 8-day averages.

We combined the in situ and satellite measurements because neither dataset spanned the entire interval of desiccation. To evaluate differences between these two datasets, we compared the temporally and spatially corresponding in situ and satellite SST observations (n = 223). For this comparison, we used in situ observations that were recorded at some time within an 8-day MCSST averaging window. In addition, we bilinearly interpolated the satellite data from the four surrounding MCSST pixels to the location where the in situ observation was taken. Over the Aral Sea, satellite SSTs are warmer than corresponding in situ SSTs by 0.4°C, with a standard deviation of 1.0°C (Fig. 4a). Because differences between the datasets are relatively small, we make no adjustment to combine the two types of measurements.

We used the combined data to estimate linear trends in SST between 1960 and 1996. Trends were calculated from all SST observations falling within windows that were 30 Julian days in duration. The analysis window was shifted 5 Julian days between successive calculations. We used SST observations from the entire sea simultaneously. An example of this regression for a window centered on 15 May is shown in Fig. 4b. The substantial SST variability in each May is the result of using a 30-day window and measurements from the entire lake. In situ measurements do not exist between January and March because the Aral Sea is partially covered by ice during this interval. Therefore, we do not estimate temperature changes for these months.

Aral SSTs increased by 4°–5°C during April and May between 1960 and 1996 (Fig. 4c). Changes during June and July are smaller (~3°C), and there is no change between August and early October. SSTs decreased in November and December by 4°–5°C. The spring and early summer increases in SST (4°–5°C) are much greater than the ~1°–1.5°C increase in air temperature observed across all of central Asia throughout the same interval (Fig. 2). In addition, SSTs have decreased while air temperatures have increased during late autumn/early winter. This suggests that large-scale climatic variability or change is not the only source of the observed changes in SST.

Considering that the individual monthly $P - E$ changes are rough estimates, the observed changes in $P - E$ and SST are consistent—$P - E$ has become more negative during months when SSTs have increased, and vice versa. This is expected because the evaporation rate is

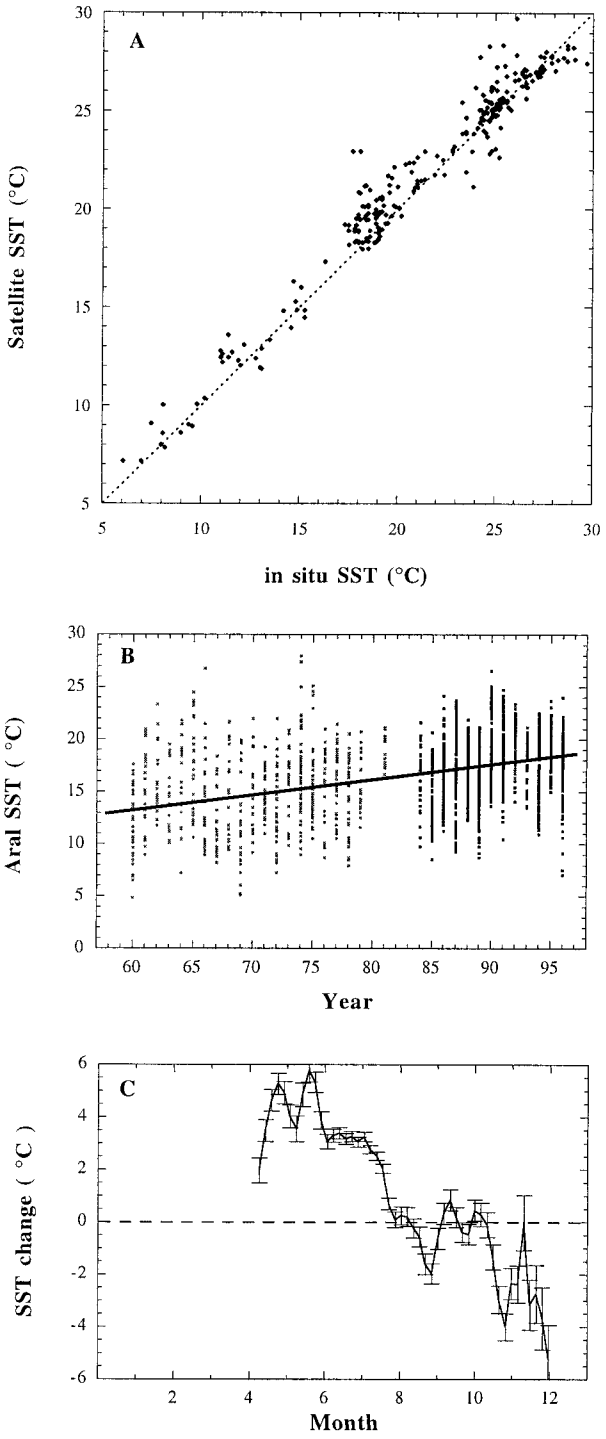

FIG. 4. (a) Comparison of temporally and spatially corresponding satellite and in situ SST observations. The dotted line is the one-to-one line. (b) In situ and satellite SST observations falling within a 30-day window centered on 15 May as a function of year (1960–97). The data prior to 1983 are only in situ measurements. After 1983, ~99% of the data are satellite measurements. The solid line is a least squares, linear fit to the data. (c) Changes in Aral SST between 1960 and 1992. Each point is plotted at the center of the 30-day window over which a linear trend was calculated. The magnitude of the change is equal to the slope determined from the linear regression times 32 yr. The error bars show 95% confidence interval estimates on the change, determined individually for each 30-day window.

strongly controlled by the temperature-dependent saturation specific humidity of the water surface.

3. Experimental design

a. Coupled regional climate–lake model

1) REGIONAL CLIMATE MODEL

We use NCAR's regional climate model (RegCM2) in this study, which is described in detail elsewhere (Giorgi et al. 1993a,b). RegCM2 is an augmented version of the Pennsylvania State University–NCAR Mesoscale Model, version 4 (MM4; Anthes et al. 1987). MM4 is a primitive equation, σ vertical coordinate, gridpoint limited-area model with compressibility according to hydrostatic balance. Some of the physics parameterizations that were added to MM4 to improve its suitability for climate studies include: 1) the convection parameterizations of Grell (1993); 2) Holtslag et al. (1990) nonlocal formulation of vertical transport in the planetary boundary layer; 3) the NCAR Community Climate Model, version 2 (CCM2) radiative transfer package, which explicitly accounts for the effects of CO_2, O_3, H_2O, O_2, and clouds (Briegleb 1992); 4) a simplified explicit cloud water scheme that prognostically calculates precipitation and cloud water for radiation calculations (Giorgi and Shields 1999); and 5) the Biosphere–Atmosphere Transfer Scheme (BATS) surface physics package (Dickinson et al. 1993).

2) LAKE MODEL

To account for the surface fluxes of heat, moisture, and momentum from the Aral and Caspian Seas, we use a lake model that is interactively coupled to RegCM2 (Hostetler et al. 1994). This model is an updated version of Hostetler and Bartlein's (1990) one-dimensional lake model that represents vertical transfer of heat by convective and eddy mixing. The improvements and additions to this model and its performance for simulating the hydrology of the Aral Sea are described in detail elsewhere (Small et al. 1999b). In this study, the lake model is used to compute: 1) Aral SSTs, 2) Aral and Caspian ice thickness and ice/snow surface temperatures, and 3) surface fluxes from both water bodies. We prescribe Caspian SSTs because a one-dimensional heat transfer approach is inadequate to represent the complex circulations in the Caspian.

Energy is transferred vertically between lake model layers ($dz = 1$ m) by eddy and molecular diffusion and by convective mixing. The eddy diffusion component represents turbulent vertical mixing, which results from

vertical gradients in the velocity of wind-induced currents (Henderson-Sellers 1985). We use the parameterization of Henderson–Sellers (1985) to calculate the eddy diffusivity at each model layer. This parameterization includes a gradient Richardson number adjustment to account for nonneutral conditions. This adjustment results in reduced eddy diffusion under stable conditions, which reduces vertical heat transfer across the simulated thermocline. Convective mixing removes density instabilities that are generated by surface heating and cooling. We use BATS version le parameterizations to calculate latent and sensible heat fluxes from the lake surface (Dickinson et al. 1993). In this bulk transfer formulation, evaporation E is proportional to the surface–air difference in specific humidity ($q_s - q_a$):

$$E = \rho_a C_D V_a (q_s - q_a), \tag{3}$$

where the subscripts a and s refer to air and surface, respectively; ρ_a is the density of air; and V_a is wind speed. The surface specific humidity is equal to the saturation specific humidity of water at the surface temperature. The momentum drag coefficient C_D is a function of the neutral drag coefficient, which depends on roughness length ($z_0 = 0.0004$ m over water), and the surface bulk Richardson number, which depends on the near-surface temperature gradient. Thus, the stability of the boundary layer affects evaporation, with unstable conditions leading to greater evaporation. The calculation of the sensible heat flux is similar to that for evaporation, except that the surface–air difference in specific humidity is replaced by the difference in temperature.

When the lake surface is ice-free, the lake surface albedo is calculated as a function of solar zenith angle (Henderson-Sellers 1986). Forty percent of the surface-absorbed shortwave radiation is absorbed within the top 0.6 m of the lake (Henderson-Sellers 1986). Absorption of the remaining shortwave radiation decreases exponentially with depth, with a scale length η constrained by observations of water transparency. Longwave radiation off the lake surface is calculated according to the Stefan–Boltzmann law, using an emissivity of 0.97.

Uniform salinity is prescribed throughout the water column and is held constant throughout each simulation. The salinities of the Caspian and Aral Seas were set at observed values. The effect of salinity on the density, specific heat, and freezing point of water are calculated according to Gill (1982). We use empirical relationships to calculate the reduction in the saturation vapor pressure over water due to salinity (Dickinson et al. 1965).

The lake model includes an ice cover scheme to represent the exchanges of heat and moisture exchanges between lake ice and the atmosphere (Patterson and Hamblin 1988). Ice growth occurs in both the open water and ice-covered fractions of a grid cell when the water temperature is at the (salinity dependent) freezing point. Ice growth does not change the salinity of the underlying water, even though salt rejection may be important in part of the Aral Sea (Bortnik 1990). A fraction of the grid cell remains open water until enough ice has formed to cover the entire grid cell to a thickness of 10 cm. The temperature profiles beneath open water and ice fractions are averaged for each grid cell.

3) LAKE–ATMOSPHERE INTERACTIONS

The lake model is interactively linked to RegCM2. At each lake model time step (30 min), air temperature, surface pressure, wind speed, specific humidity, precipitation, and downward short- and longwave radiation from the lowest atmospheric model level are passed to the lake model. Based on these meteorological inputs and the lake surface temperature and albedo, the lake model calculates the lake–atmosphere exchanges of moisture, heat, and momentum. The lake surface energy balance is then calculated from these quantities. The lake surface temperature and the temperature profile within the lake are adjusted according to the surface energy balance.

There is a single lake model vertical column for each RegCM2 grid cell in which the BATS land cover category is specified as ''lake.'' There is no transfer of heat or other quantities between adjacent lake points. As shown in Small et al. (1999b), this approach is adequate to simulate the hydrologic processes of the Aral Sea.

b. Model domain

The model domain used here has a resolution of 50 km, covers a 3400 km $\times$ 3100 km area, and includes the entire Aral Sea drainage basin (Fig. 1). BATS land cover categories were set using Olsen's 30-min global ecosystem dataset. The only areas of surface water within the domain are the Caspian and Aral Seas, as well as some wetlands along the northern and eastern boundaries. The Aral Sea is surrounded by desert, except on the northern side where grasslands predominate. Cropland is present along the Amu Darya and throughout the Amu Darya delta.

c. Model experiments

1) ARAL SEA SENSITIVITY EXPERIMENTS

We completed three continuous 5.5-yr-long simulations, varying the characteristics of the Aral Sea in each experiment. The purpose of these simulations is to examine the effects of changes in Aral Sea size, depth, and salinity. All three simulations were driven by the same time-dependent lateral boundary conditions. Wind, temperature, water vapor, and surface pressure were derived from 12-h European Centre for Medium-Range Weather Forecasts (ECMWF) analyses on a T42 spectral grid (Trenberth 1992), for the period 1 June 1987 through 1 January 1993. These boundary conditions were applied over a 400-km buffer zone along the

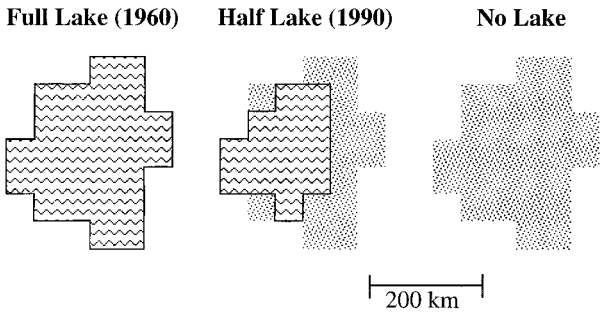

FIG. 5. Schematic of the Aral Sea as represented in the lake size sensitivity experiments. The wavy pattern denotes water surface and the dotted pattern desert.

lateral boundaries of the domain (Fig. 1). Time-dependent Caspian SSTs were prescribed according to the 50 km × 50 km resolution Pathfinder AVHRR SST dataset.

In the first two experiments, the surface area, depth, and salinity of the Aral Sea were prescribed according to the observed values in 1960 and 1990 (Table 1). We refer to these simulations as the ''Full Lake'' (1960) and ''Half Lake'' (1990) experiments, and they represent predesiccation and conditions in 1990, respectively. The Aral Sea covers 28 model grid cells in the Full Lake case and 14 model grid cells in the Half Lake case. The ''desiccated'' grid cells are prescribed to be desert, because this represents the environmental change that has accompanied desiccation (Micklin 1988). The sea-averaged depth decreased by nearly half between 1960 and 1990 (Table 1). In each simulation, the depth at each model cell was set to the mean depth for the area covered by that cell, as calculated from ~1-km resolution bathymetry (R. Ressl 1996, personal communication) and the observed sea level at that time. The salinity increased from 10 to 33 ppt between 1960 and 1990, resulting in a depression of the freezing point from $-0.5°$ to $-1.8°$C.

In both the Full and Half Lake experiments, the exponential lengthscale η over which shortwave radiation is absorbed was varied spatially according to observed Secchi Disc depth measurements (Bortnik 1990), and empirical relationships between Secchi Disc measurements and η (Graham 1966). In both experiments, we initialized the lake temperature profile at each lake point by driving the lake model with 6-h inputs derived from the International Satellite Land Surface Climatology Project (ISLSCP) dataset. Two years of ISLSCP data (1987–88) were repeatedly input to the lake model until temperature at the deepest lake points stopped changing, which took ~10 yr. Temperature profiles from 1 June 1987 were then used to initialize the coupled model. We exclude the first 7 months of the coupled simulation (June–December 1987) from all analyses to minimize possible problems associated with model spinup, leaving five complete years for analysis (1988–92).

In the third experiment, the Aral Sea was completely removed and replaced by desert (Fig. 5). This simulation is referred to as the ''No Lake'' experiment.

Differences between the Full and No Lake experiments are the result of replacing the Aral Sea by desert, as all other boundary condition used in the two simulations are identical. We use these differences to examine how the Aral Sea influences the climate over the sea and in the surrounding region (Table 2). Differences between the Full and Half Lake experiments are the result of the changes in Aral Sea characteristics. We use these differences to examine how $P - E$ and SSTs would change as the result of desiccation between 1960 and 1990 (Table 2). The simulated changes are compared to the observed hydrologic changes that have accompanied desiccation during this interval. Internal model variability may also introduce changes between the various experiments. These differences are likely negligible because the evolution of each simulation is constrained by the time-dependent meteorological boundary conditions. The effects of internal model variability are discussed below (sections 4 and 5).

The Half Lake simulation is the only case in which the characteristics of the Aral Sea (1990 values) cor-

TABLE 2. (top) The Aral Sea characteristics and meteorological boundary conditions used in the four experiments examined in this study. (bottom) The comparisons made between the various experiments, the difference between the experiments, and what the comparisons are designed to represent.

Experiment	Aral Sea characteristics	Meterological boundary conditions
Full Lake	1960 (predesiccation)	1987–92
Half Lake	1990	1987–92
No Lake	None	1987–92
Cold	1960 (predesiccation)	1991–92 with 1.5° cooling

Comparison (expt A − B)	Difference between expt A and expt B	Used to investigate:
Full Lake − No Lake	1960 Aral Sea vs desert	Influence of the Aral Sea on climate
Half Lake − Full Lake	1990 Aral Sea vs 1960 Aral Sea	Hydrologic effects of desiccation (1960–90)
Full Lake − Cold	''Warm'' vs ''Cold'' meteorological boundary conditions	Hydrologic effects of warming (1960–90)
Half Lake − Cold	1990 Aral vs 1960 Aral ''Cold''	Combined effects of desiccation and warming between 1960 and 1990

TABLE 3. Observed and simulated (Half and Full Lake) components of the Aral Sea water balance. Simulated precipitation, evaporation, and $P - E$ are calculated over the Aral Sea only. The observed precipitation is the average value from the 1000 km $\times$ 1000 km area surrounding the Aral Sea in the Legates and Willmott climatology (1990). All units: mm yr^{-1}. Maximum estimate of the observed evaporation and the corresponding minimum estimate of $P - E$ are included, based on water balance calculations.

	Precipitation	Evaporation	$P - E$
Observations (1988–92)	212	1216 (max)	−1004 (min)
Model (Half Lake)	253	1081	−828
Model (Full Lake)	244	1031	−787
Simulated change: Half − Full	9	50	−41
Observed change			−141

respond with the temporally varying meteorological boundary conditions (1988–92). By comparing results from the Half Lake simulation with temporally corresponding meteorological and hydrological observations, we have demonstrated that the coupled RegCM2-lake model accurately simulates the hydrologic behavior of the Aral Sea (Small et al. 1999b). The annual precipitation and evaporation simulated by RegCM2 are similar to observed values (Table 3). However, the simulated evaporation is greater than observed during summer and less than observed during winter. The lake model coupled to RegCM2 accurately reproduces Aral Sea SSTs, with a mean bias of only −0.5°C. In addition, the lake model also simulates the observed midwinter ice fraction well, although the onset of ice growth occurs too late in the year and the ice melts too rapidly in the spring.

2) CLIMATE CHANGE EXPERIMENT

We completed an additional experiment to examine the influence of observed large-scale warming since 1960 (Fig. 2) on the hydrologic conditions of the Aral Sea. Using the method of Schar et al. (1996), we represented the cooler, predesiccation air temperatures by perturbing the same ECMWF boundary conditions used in the lake size experiments. The Aral Sea characteristics were specified at the predesiccation (Full Lake) values (Table 1). The perturbation in this ''Cold'' experiment included 1) a decrease in temperature of 1.5°C and 2) and a decrease in the specific humidity so that the relative humidity was unchanged (Table 2). The perturbation was applied at each model level and throughout the entire buffer zone over which the boundary conditions are applied. This perturbation does not alter horizontal pressure gradients within the buffer zone, so the external flow field is unmodified and the change at the domain boundaries is purely thermodynamic (Schar et al. 1996). Therefore, any external dynamical forcing that has occurred since 1960, such as changes in winds driven by the NAO, is not represented. The assumption of constant relative humidity is based on studies that show that midlatitude temperature variations are generally accompanied by minimal changes in relative humidity (Schar et al. 1996). For a change of 1.5°C, the decrease in water vapor content throughout the domain examined here is 5%–10%, depending on the season.

We initialized the Cold experiment from the Full Lake (1960) simulation, starting in July 1989. The same perturbations discussed above were applied to create the initial meteorological fields. Soil temperature and Caspian and Aral SSTs (full vertical profiles) were also lowered by 1.5°C. The Cold experiment is 2.5 yr in duration. The entire interval overlaps with the lake size experiments (Table 2). As for the lake size simulations, we excluded the first 6 months of this experiment to minimize spinup effects.

We designed the Cold experiment to assess the hydrologic response of the Aral Sea to the observed large-scale warming between 1960 and the mid-1990s. We used a temperature perturbation of 1.5°C to ensure a substantial model response, even though this change is greater than the warming observed during spring and fall (Fig. 2). Therefore, this experiment should provide a maximum estimate of changes that may have resulted from large-scale forcing. The effects of enhanced greenhouse gas concentrations on the global climate system may be one source of the observed regional warming. However, the change in trace-gas radiative forcing within our domain is only ~1 W m^{-2} between 1960 and the mid-1990s (Kiehl and Briegleb 1993). We do not include this negligible radiative effect in the Cold experiment.

We did not use ECMWF analyses from 1960 to represent the cooler conditions prior to desiccation. The simulated response would depend strongly on the particular years chosen for boundary conditions because interannual temperature variability is substantial in central Asia (Fig. 2). In addition, changes in the ECMWF model or the data available for assimilation may have introduced changes unrelated to warming. A more ''realistic'' experiment would be to complete a continuous simulation from 1960 through 1995, but this was not feasible given available computing resources.

Differences between the Cold and Full Lake experiments are due to the perturbation of the boundary and initial conditions, and perhaps internal model variability. We use the differences between these simulations (Full minus Cold) to examine how large-scale warming would influence the Aral Sea (Table 2). To examine the combined effects of warming and desiccation, we compare the Cold and Half Lake experiments. These experiments differ in terms of both the temperature per-

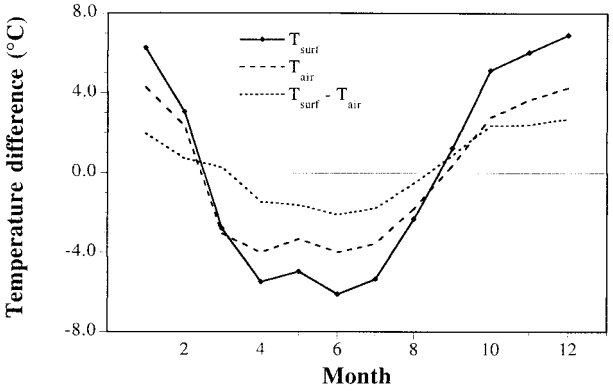

FIG. 6. Full minus No Lake differences of surface temperature (solid), 2-m air temperature (dashed), and surface–air temperature difference (dotted) by month. Values are averaged over the Aral Sea and the 5-yr of the simulation.

turbation and the characteristics of the Aral Sea (Table 2). For the comparisons that include the shorter Cold experiment, we calculated differences only for the 2-yr interval that is common to the Full Lake, Half Lake, and Cold simulations (1990–1991).

4. Lake–atmosphere interactions

In this section, we explore how interactions between the Aral Sea and the atmosphere affect the climate of the surrounding region. This is useful for understanding the effects of desiccation on the hydrologic conditions of the sea. We assess the simulated lake–atmosphere interactions by comparing the Full and No Lake experiments. The differences between these two simulations are due to replacing the Aral Sea with desert (Table 2). We compare the Full and No Lake experiments, rather than the Full and Half cases, because complete removal of the Aral Sea allows for the most straightforward assessment of the simulated lake effect.

a. Temperature changes

1) SURFACE TEMPERATURE

The simulated climatic effects of the Aral Sea are driven by the thermal contrast between the lake and adjacent land surfaces. When compared with the desert land surface in the same location (Fig. 5), Aral SSTs are cooler by up to 6°C between March and August, and warmer by up to 7°C between September and February (Fig. 6). Differences in air temperature over the lake are of the same sign, but decrease in magnitude with distance from the ground (Fig. 6). The Aral Sea also modifies the surface-to-air temperature gradient, and therefore the near-surface stability of the atmosphere. When compared with the No Lake experiment, the boundary layer is more stable during spring and summer and less stable in autumn and winter, as indicated by the difference between the surface and 2-m air temperatures (Fig. 6).

The seasonal cycle of lake surface temperature lags behind that of the land surface by several months because the lake has greater thermal inertia. During spring and early summer, ~100 W m^{-2} more energy is transferred from the atmosphere to the lake surface than from the atmosphere to the land surface (Fig. 7a). This contrast exists because the albedo and moisture availability of the lake and the land surface are substantially different. Even though more energy ''enters'' the lake from the atmosphere, the land surface heats up more rapidly (Fig. 6) because its surface energy balance (SEB) is more positive (Fig. 7b). Most of the energy transferred form the atmosphere to the lake immediately passes through the surface layer. The energy flux from the lake's surface layer to the underlying water column nearly equals the atmosphere-to-surface flux and is an order of magnitude greater than the equivalent ''ground heat flux'' over land (Fig. 7c). The result is that much more energy is stored beneath the lake surface on the seasonal timescale. Two processes are critical: 1) heat is transferred efficiently throughout the water column by eddy and convective mixing; and 2) shortwave radiation penetrates deeply into the water (with an *e*-folding depth of ~4 m). The process of seasonal heat storage is reversed during the fall and winter. The simulated lake effect exists because the lake acts as an energy sink (source) in the spring and summer (autumn and winter), similar to the results of Lofgren (1997). Changes in lake depth influence seasonal energy storage and therefore the intensity of the lake effect—a shallow lake will behave more like the land surface.

2) MEAN AIR TEMPERATURE

The Aral Sea has the greatest influence on air temperature in the surrounding region when the lake–land temperature contrast is greatest (October–January and April–July) (Fig. 6). During January, the relatively warm lake surface heats the overlying air primarily through the transfer of sensible heat. The warm air over the lake is advected to the east by the simulated prevailing winds, resulting in a modest warming that extends for ~250 km downwind of the Aral and vertically to ~850 mb geopotential height (1.5 km) (Fig. 8). The magnitude of the lake-to-land temperature contrast, however, is not the only important factor determining the strength of the lake effect. During October, both the lake–land temperature contrast (Fig. 6) and the atmosphere-to-lake energy transfer (Fig. 7a) are similar to the January values. However, increases in surface air temperature beyond the shoreline are negligible (Fig. 8) and the warming extends only to 950-mb geopotential height (200 m) in October. Temperature changes are minor during October because the latent heat flux accounts for nearly all of the energy transferred from the lake surface to the atmosphere and only a small fraction

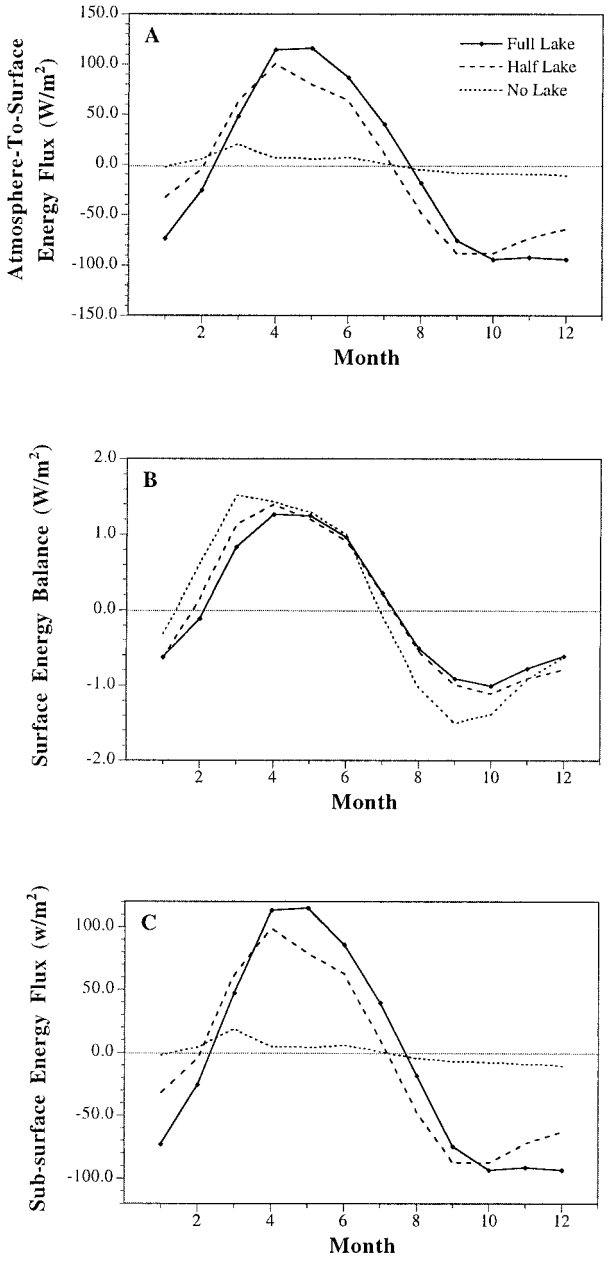

FIG. 7. (a) Monthly atmosphere-to-surface energy transfer (net radiation minus the sum of the sensible and latent heat fluxes) over the Aral Sea from the Full (solid line), Half (dashed), and No Lake (dotted) experiments. In the No Lake experiment, the surface energy balance is calculated over the area covered by the Aral Sea in the Full Lake case. Positive values indicate energy is being transferred from the atmosphere to the lake or land. (b) The surface energy balance (for the top 10 cm) of the lake or land surface. (c) Total energy flux from the surface layer (10 cm) to the underlying water or soil column [equal to (a) − (b)]. This transfer reflects a combination of shortwave penetration, convective mixing, and eddy diffusion in the lake and only conduction for the land surface. All values are averaged over the five simulated years.

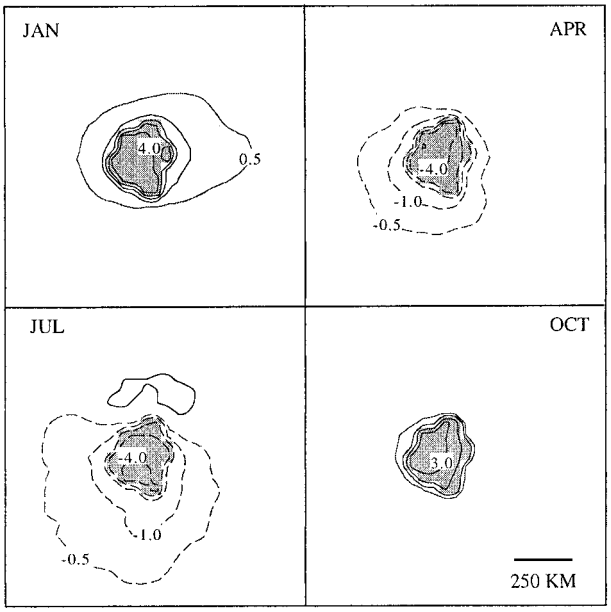

FIG. 8. Two-meter air temperature difference between the Full and No Lake simulations in Jan, Apr, Jul, and Oct. The contour interval is 1°C, with contours for −0.5 and 0.5°C also included (gray). Solid lines denote positive differences (Full > No Lake) and dashed lines denote negative differences. Only a portion of the model domain is shown. The gray shaded region is the Aral Sea. Values are averaged over the five simulated years.

of the evaporated lake water condenses locally heating the air around the lake.

The Aral Sea cools the air in the surrounding region during spring and summer (Fig. 8). In the No Lake experiment during July, nearly all of the net radiation absorbed by the desert surface is balanced by sensible heating of the overlying air. In contrast, the net radiation absorbed by the lake surface in the Full Lake case is balanced by heating throughout the water column and evaporation. Neither process warms the overlying air, resulting in relatively cool air temperatures over the lake. This cool air is advected by the prevailing, northeasterly surface winds. Cooling of >0.5°C extends up to 400 km from the southern shore of the lake (Fig. 8) and extends to 750-mb geopotential height (2.0 km).

In most months, replacing the Aral Sea with desert has a negligible effect on the energy balance (<1 W m^{-2}) of the land surface around the lake. One notable exception is that shortwave radiation is enhanced to the north of the lake in the Full Lake experiment, which yields warmer temperatures (Fig. 8). The increased shortwave radiation results from a reduction in cloud cover, driven by near-surface divergence and locally descending air. Two different observations suggest the simulated warm–cool summertime pattern is realistic (Fig. 8). An equivalent reduction in summertime cloud cover is observed on the upwind side of lakes in the Great Lakes region (Eichenlaub 1970). In addition, Small et al. (2001) found that summer air temperature

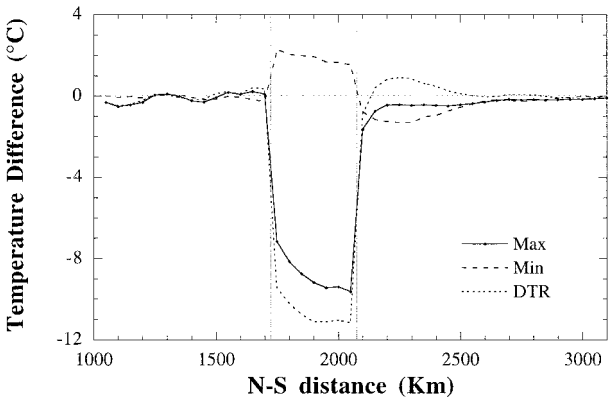

FIG. 9. Full minus No Lake differences of 2-m air temperature in Jul: daily maximum (solid), daily minimum (dashed), and DTR (dotted). A cross section from North to South across the Aral Sea is shown, averaged over an East–West width of 150 km. The vertical solid lines show the North and South edges of the Aral Sea. The *x* axis is labeled in kilometers from the northern edge of the domain. Values are averaged over the five simulated Julys.

was warmer to the north of the Aral Sea prior to desiccation, even though cooler conditions existed both over and to the south (downwind) of the lake.

3) DIURNAL TEMPERATURE RANGE

The thermal inertia of the Aral Sea also influences daily temperature extremes, and therefore the diurnal temperature range (DTR). The greatest change in temperature extremes occurs during summer, when intense shortwave heating of the desert land surface results in the largest DTR. During July, for example, the maximum daily air temperature is reduced by ~10°C over the sea, by ~1°C to the south of the sea, and is unchanged to the north (Fig. 9). Minimum temperatures increase by ~2°C over the sea and decrease by a smaller amount to the south of the shoreline (Fig. 9). Increased daytime cloudiness and advection of cool air from over the lake are the sources of the latter change. The net result is a 10°C reduction of the DTR over the lake and a slight increase south of the shoreline (Fig. 9).

The influence of the Aral Sea on temperature extremes is reversed during the cold season—increases in minimum temperature are greater in magnitude than the increases in maximum temperature. Over the lake, maximum temperature increases by only ~3°C whereas minimum temperature increases by up to 8°C, yielding a reduction of the DTR by ~5°C. Changes beyond the shoreline are relatively minor (<1°C), similar to the summertime result.

4) COMPARISON TO OBSERVED CHANGES IN AIR TEMPERATURE

Small et al. (2001) identified changes in surface air temperature resulting from desiccation between 1960 and 1997. These changes can be used to assess the simulated response to replacing the Aral Sea by desert. An exact match is not expected because the actual and simulated forcings differ, partial versus complete desiccation, respectively. The following features of the simulated and the observed changes are similar: 1) the magnitude and annual cycle of mean temperature changes over the lake; 2) the spatial extent and pattern of changes beyond the lake shoreline, including the warming north of the Aral during July (Fig. 8); 3) enhanced changes in maximum (minimum) temperature during spring and summer (fall and winter); and 4) increased DTR in all seasons. An important difference does exist. The magnitude of simulated changes in both mean and extreme temperatures is typically less than observed beyond the 1960 lake shoreline, even though the simulated disturbance encompasses a greater area. The representation of boundary layer processes or the coarse model resolution may contribute to this discrepancy. Overall, the model closely reproduces the temperature response to desiccation. This suggests that it is reasonable to use the model as a tool to investigate the changes in lake–atmosphere interactions and lake hydrologic conditions resulting from desiccation.

b. Dynamical changes

The temperature difference between the lake and adjacent land surface generates a sea-breeze circulation, as shown by differences in the wind fields between the Full and No Lake experiments. The intensity of the sea breeze primarily scales with the lake-to-land contrast in sensible heating, and is therefore greatest during the daytime hours of the summer months.

We demonstrate the simulated dynamical effects of the Aral Sea using the example of July. At 0700 Local Standard Time (LST), the sea does not influence the local winds because the surface temperature of the water is similar to that of the adjacent land surface. In comparison with the sea surface, the land surface warms rapidly throughout the morning. The warm land surface then heats the overlying air via sensible heat transfer, generating a sea-to-land pressure gradient at ~800 mb geopotential height. The resulting flow toward the sea yields low surface pressure over land and high surface pressure over the water. The sea breeze (lake-to-land) is driven by this surface pressure difference.

During July, the sea breeze is most intense in midafternoon when the sea-to-land thermal contrast is >8°C and extends upward to ~800 mb geopotential height (Fig. 10a). The sea breeze, which blows from lake-to-land in all directions, extends from the surface to 900-mb geopotential height with peak velocities of ~3.5 m s^{-1} directly over the shoreline (Figs. 10b and 10c). The return flow is slower and more diffuse, extending from 900 to ~600-mb geopotential height with a velocity of ~1 m s^{-1}. Over the Aral Sea, divergence near the surface and convergence at ~700-mb geopo-

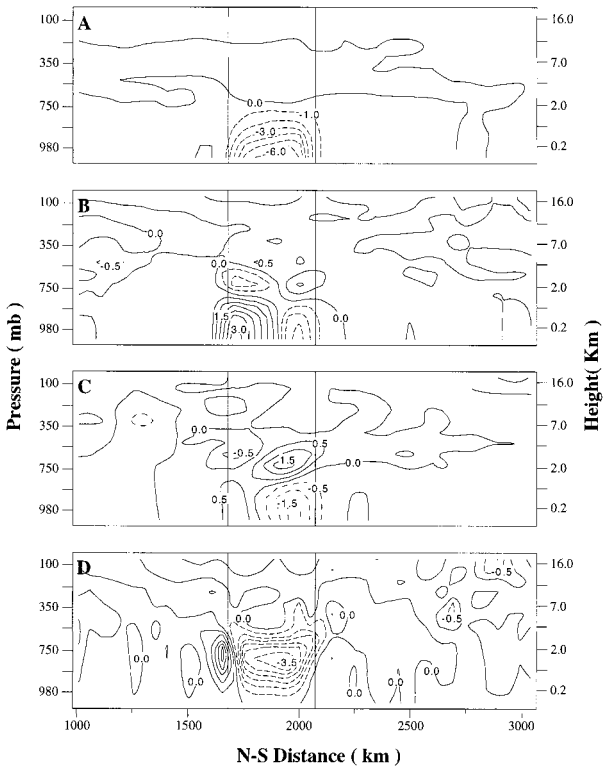

FIG. 10. Vertical cross section (N–S) across the Aral Sea at 1600 LST during Jul, averaged over the five simulated years. Panels show Full minus No Lake differences of: (a) air temperature (°C), (b) N–S wind velocity (positive is north); (c) E–W wind velocity (positive is east); and (d) vertical wind velocity (positive is up). The units of horizontal wind differences are meters per second and vertical wind differences are centimeters per second. The cross section shows values averaged over an East–West width of 150 km. The north and south shorelines of the Aral Sea are shown by the vertical lines. The *x* axis is labeled in kilometers from the northern edge of the domain.

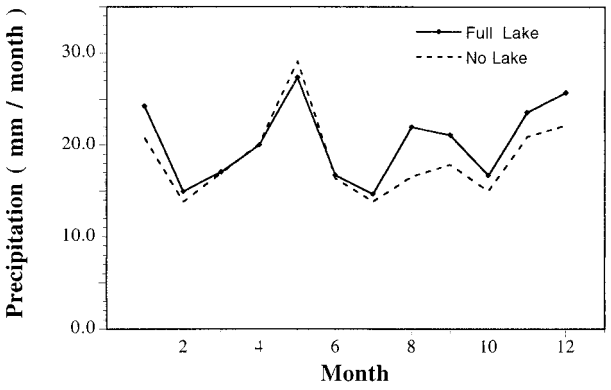

FIG. 11. Monthly precipitation over the Aral Sea in the Full (solid) and No Lake (dashed) simulations, averaged over 5 yr. In the No Lake simulation, precipitation is averaged over the area covered by the sea in the Full Lake experiment.

tential height results in descending air (Fig. 10d). The reverse is true over the land directly adjacent to the shore. Peak descending and ascending velocities are 3 cm s^{-1}. The vertical extent and intensity of the simulated circulation are similar to observed values for sea breezes in other locations (Atkinson 1981). The intensity of the sea breeze decreases substantially after 2200 LST as the thermal contrast diminishes.

Two additional features of the simulated circulation are similar to sea breezes observed elsewhere. First, the northern cell of the sea breeze is stronger than the southern cell (Fig. 10b). The background flow is from the north at this time of day, which enhances (reduces) the temperature contrast along the northern (southern) shoreline strengthening (weakening) the sea breeze (Pielke 1984). Second, during the afternoon (1600 LST), the thermally driven flow is stronger across the shoreline (across isobars) than parallel to it. Throughout the afternoon and evening, the simulated sea-induced winds shift to flow parallel to the shorelines (along isobars), again matching observations from other locations (Atkinson 1981). This directional shift is due to the adjustment to geostrophy.

A sea breeze similar to that simulated in July exists between May and October, although it is weaker in intensity. During the cold season, when the sea is warmer than the adjacent land, a weak land breeze develops near the surface. This land breeze results in near-surface convergence and rising air over the Aral Sea. In all seasons, the circulation driven by the sea–land thermal contrast influences the hydrologic budget of the sea. During the summer, evaporation from the sea is enhanced by the descending motion, which advects dry, warm air toward the sea surface. The effects of the sea breeze on precipitation are now described.

c. Precipitation

1) AUTUMN AND WINTER

We define lake-effect precipitation to be the difference between the precipitation in the Full and No Lake experiments. The Aral Sea enhances on-sea precipitation between October and February (Fig. 11), when the sea surface is warmer than the adjacent land (Fig. 6). During the cold season, the simulated lake-effect precipitation is greatest during December and January. During these months, precipitation increases by greater than 20% over the sea and by a lesser amount (<10%) to the east of the shoreline (Fig. 12a).

During the cold season, the simulated pattern of lake-effect precipitation is similar to that observed near the Great Lakes. However, the magnitude is much less than the 30%–50% increase observed downwind of each of the Great Lakes (Eichenlaub 1970). Is lake-effect precipitation actually less around the Aral Sea or does this difference reflect model shortcomings? It is not possible to actually measure Aral Sea lake-effect precipitation because the network of meteorological stations around the Aral Sea is too sparse (Small et al. 2001). Some mesoscale lake–atmosphere processes are not resolved

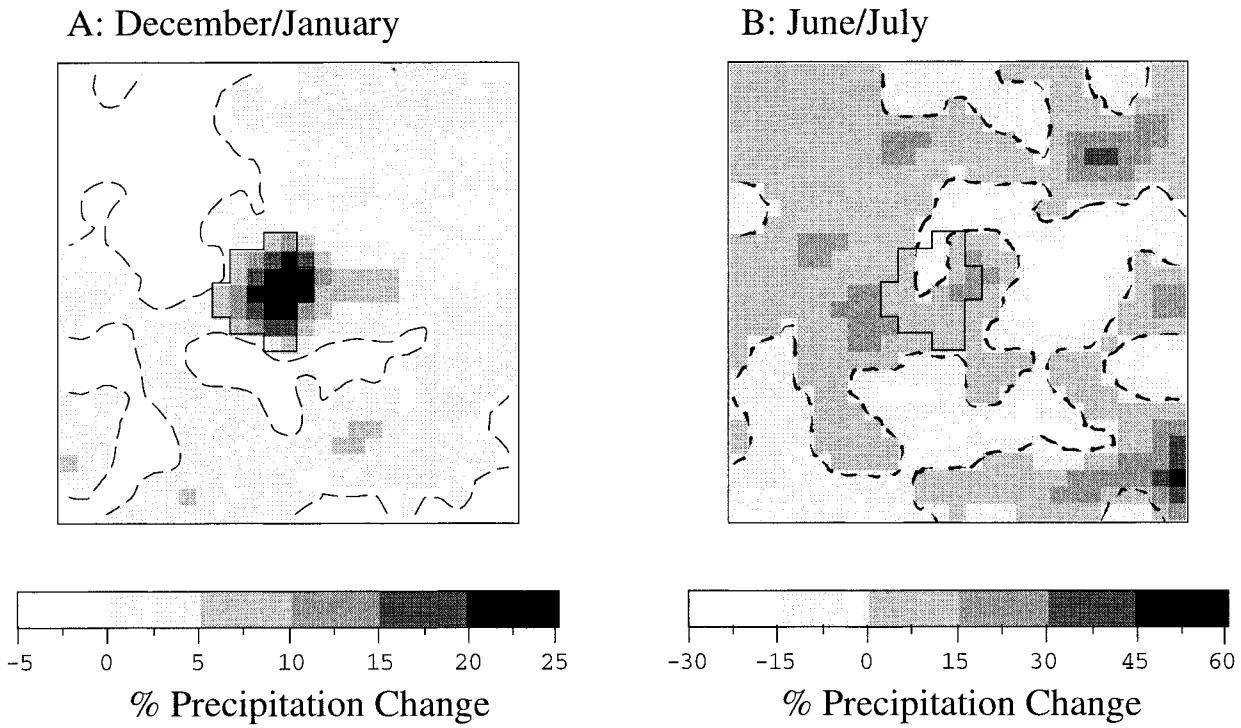

FIG. 12. Percent precipitation difference between the Full and No Lake experiments in (a) Dec–Jan and (b) Jun–Jul averaged over 5 yr.

at 50-km resolution. However, this is probably not the source of the limited lake-effect precipitation simulated by the model. Bates et al. (1995) used an earlier version of the RegCM-lake model with both 60- and 30-km resolution for a domain including the Great Lakes and found lake-effect precipitation slightly greater than observed values. In order to assess whether the simulated lake-effect precipitation is accurate, we are restricted to examining if the processes that limit the lake-effect precipitation are reasonable.

The mechanism that produces cold season lake-effect precipitation in the Full Lake case is similar to that observed (Niziol et al. 1995; Ellis and Leathers 1996) and modeled (Hjelmfelt 1990; Hsu 1987) for the Great Lakes. This is demonstrated by a series of cold season storms passing over the eastern margin of the lake (Fig. 13). The highest precipitation rates in both the Full and No Lake experiments occur during the passage of cold fronts: peaks in precipitation intensity are correlated with sea level pressure minima (Figs. 13a and 13b), temperature maxima, and shifts from southeasterly to northwesterly surface winds. The difference between precipitation in the two experiments is greatest following frontal passage during the subsequent periods of rising surface pressure, as is the case for the Great Lakes (Fig. 13c) (Ellis and Leathers 1996).

In the No Lake experiment, it takes ~1 day after the passage of a front for the cold, dry air advected from the north to lower the temperature of the land surface. During this period, the combination of the warm surface and cold, dry air aloft results in a negative gradient of equivalent potential temperature, θ_e (Fig. 13d). We focus on the difference between the surface and ~900-mb geopotential height because this is the typical height of the lifting condensation level during the winter.

In the Full Lake experiment, the negative θ_e gradient is stronger and persists longer following the passage of each front (Fig. 13d). This is the case because 1) the relatively high thermal inertia of the lake surface buffers the reduction of surface temperature subsequent to cold front passage, and 2) evaporation from the sea surface accentuates the vertical specific humidity gradient. The negative θ_e gradient in the Full Lake case persists until the warm, moist air associated with the subsequent low pressure system reaches the Aral Sea. In each case of lake-effect precipitation (Fig. 13d), the vertical gradient in θ_e is negative, indicating the presence of a convective instability. For this potential instability to be released, the surface air must be raised above its lifting condensation level, which is typically at a geopotential height of ~900 mb or greater. In the Full Lake experiment, near-surface convergence and lifting results from 1) frictional convergence on the downwind shoreline and 2) the land breeze driven by the lake–land thermal contrast.

As compared with December and January, lake-effect precipitation is less in other months of the cold season (Fig. 11). The lifting condensation level is often above 750-mb geopotential height during fall. Therefore, mesoscale lake-effect convergence is not sufficient to release the severe potential instability that exists during

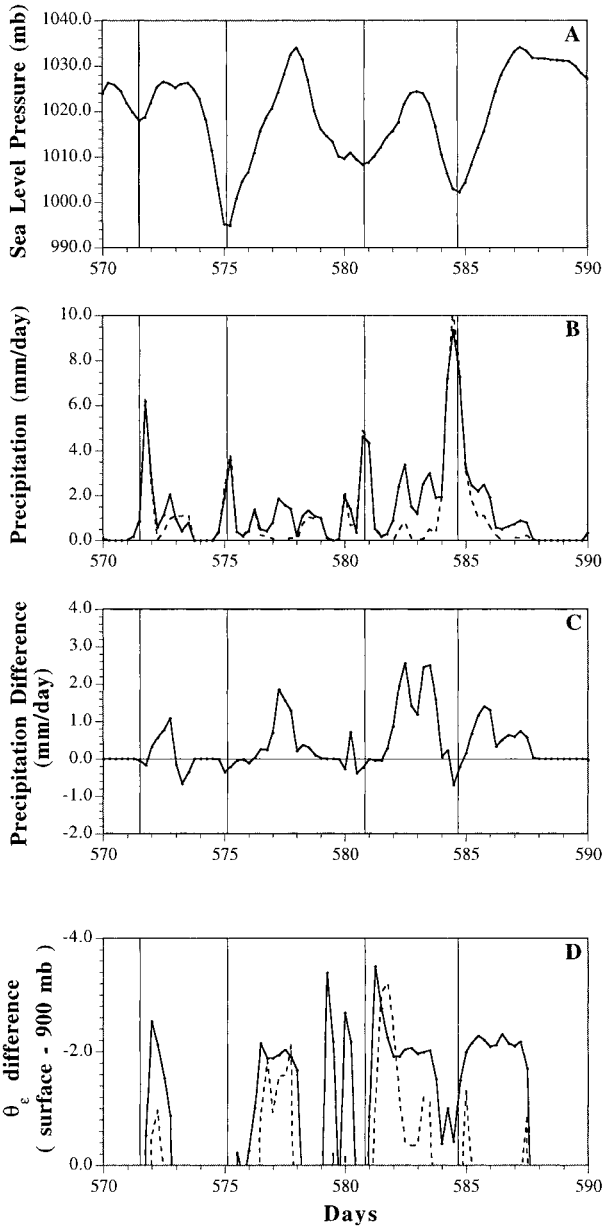

FIG. 13. Twenty-day times series for a single grid cell at the eastern edge of the Aral Sea: (a) sea level pressure in the Full Lake experiment; (b) precipitation rate (mm day^{-1}) in the Full (solid) and No (dashed) Lake experiments; (c) Full minus No Lake precipitation difference; and (d) the difference (°C) in equivalent potential temperature θ_e between the surface and ~900 mb, in the Full (solid) and No (dashed) Lake experiments. Values are plotted every 6 h. The vertical solid lines mark the pressure minima. The *x* axis is labeled in days since the start of the simulation.

this season. After January, lake-effect precipitation is minimal because Aral Sea ice cover reaches nearly 80%. We completed a 6-month winter simulation in which Aral SSTs were constrained to stay above the freezing point so that ice did not form. In this sensitivity experiment, precipitation over the ice-covered portion of the sea increased by 30%–50%.

We propose that lake-effect precipitation around the Aral Sea is less than that observed around the Great Lakes for two reasons. First, there is no elevated topography around the Aral Sea. Downwind of the Great Lakes, however, topography has been shown to enhance lake-effect precipitation by lifting the surface air and releasing convective instabilities (Hjelmfelt 1992). Second, during late fall and winter, Aral SSTs are cooler and ice fractions greater than for the largest Great Lakes because the Aral Sea is relatively shallow. This decreases the sea-to-land temperature contrast limiting the ''lake-effect'' precipitation.

2) SPRING AND SUMMER

Aral SSTs are cooler than the adjacent land surface temperatures from March until September (Fig. 6). However, the difference in on-lake precipitation between the Full and No Lake experiments is not consistent throughout this part of the year (Fig. 12). In comparison with the No Lake experiment, on-lake precipitation in the Full Lake simulations is reduced or unchanged in the spring and is enhanced between June and September, with the greatest increase (30%) during August. Unlike the winter months, the pattern of precipitation changes that result from replacing the Aral Sea with desert includes areas of positive and negative change (Fig. 12b).

During the summer, θ_e is greater by up to 10°C over the Aral Sea in the Full Lake experiment because of the increase in humidity from lake evaporation. On most days, the resulting convective instability is not released because the sea-breeze leads to descending air over the lake (Fig. 10). Under these conditions, the Aral Sea reduces precipitation over the lake. However, the sea breeze and associated descending air do not develop on relatively cool and cloudy days. The combined effects of the warm and wet conditions near the surface and the lack of descending air yields intense precipitation events. Averaged over all days, changes in precipitation over the Aral Sea are small (Fig. 11)—the reduction of precipitation on most days is balanced by the substantial enhancement on the less frequent, cooler days. In August, the lake–land thermal contrast is minimal (Fig. 6), but the near-surface specific humidity is very high because Aral Sea evaporation is greatest during this month. Therefore, precipitation is enhanced the most during this month.

During the summer, the Aral Sea enhances (reduces) precipitation to the north and west (south and east) of the sea (Fig. 12b). Internal model variability is one source of the spatial variability in precipitation changes. However, the northwest–southeast pattern is consistent with the changes expected to result from interactions between the lake-induced circulations and the large-scale wind. The sea breeze and northwesterly synoptic wind converge to the north and west of the Aral Sea, leading to rising air and enhanced precipitation. In con-

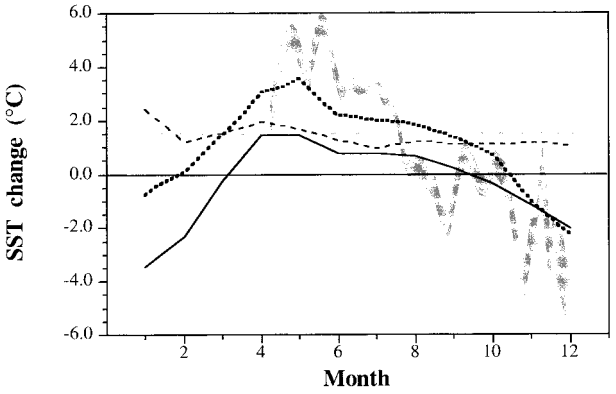

FIG. 14. Simulated, monthly averaged SST change from desiccation (Half − Full: solid), warming (Full − Cold: dashed), and the combination of desiccation and warming (Half − Cold: dotted). The gray shaded area shows the observed SST change between 1960 and 1992, including the 95% confidence interval estimate. The horizontal gray line shows the expected warming from the boundary condition perturbation in the Cold experiment (1.5°C). The Half − Full difference is a 5-yr average and the others are 2-yr averages.

trast, the lake breeze enhances the large-scale wind to the southeast of the sea, resulting in divergence and a reduction in precipitation.

The simulated enhancement of on-lake precipitation in the Aral Sea region begins earlier in the summer than observed for the Great Lakes (Miner and Fritsch 1997). In addition, the magnitude of lake-effect precipitation is somewhat greater. These differences likely exist because Aral SSTs are warmer and evaporation greater during the summer than for most of the Great Lakes, primarily because the Aral Sea is relatively shallow.

5. Influence of desiccation

We now examine how desiccation between 1960 and the mid-1990s influenced the water balance and surface temperature of the Aral Sea by comparing the Full and Half Lake experiments. The previous comparison (Full vs No Lake) provides no information about the hydrologic effects of desiccation because the sea is completely removed in the No Lake simulation. We present modeled differences as Half minus Full Lake because this is consistent with the direction of changes that would occur as the lake dries up (Table 2). These differences are then compared to the observed $P - E$ and SST changes.

a. SST changes

There are substantial differences in SST between the Half and Full Lake experiments. Between April and October, SSTs are warmer in the Half Lake case, with a maximum difference of 1.5°C in April (Fig. 14). Half Lake SSTs are cooler by up to 3.5°C throughout the remainder of the year. These SST differences between the two experiments are the result of changes in lake depth, salinity, and atmospheric conditions over the lake, the latter which represents the influence of changes in lake–atmosphere interactions.

Aral SSTs in the Half Lake case warm relative to those in the Full Lake case between January and April (Fig. 14). During this interval (except April), the atmosphere-to-surface energy flux is more positive in the Half Lake experiment—colder SSTs result in greater sensible heating of the surface and reduced cooling via evaporation and emission of longwave radiation. The extra energy added to the Half Lake surface results in both faster warming of the surface layer (i.e., a more positive SEB) (Fig. 7b) and additional energy storage beneath the lake surface (Fig. 7c).

Throughout the remainder of the year, Half Lake SSTs cool in comparison with the Full Lake SSTs (Fig. 14). Between April and September, ~25% less energy is stored (per unit area) beneath the surface layer in the Half Lake case (Fig. 7c) because the thermocline intercepts the bottom of the shallow lake earlier in the year than it does in the deep lake. Between October and January, the atmosphere-to-lake energy transfer in the Half Lake experiment is less negative (Fig. 7a) but the SSTs continue to cool relative to the Full Lake case. During these months, convective mixing releases the additional energy stored in the deeper Full Lake water column (Fig. 7c), which keeps the SEB more positive and the surface layer warmer.

The simulated SST changes between the Full and Half Lake experiments are similar to the observed changes that have accompanied desiccation (Fig. 14). Both simulated and observed SSTs are warmer between April and August, are unchanged during the late summer/early fall, and are colder between October and December. However, the magnitude of simulated SST changes is less than observed, particularly between May and July. There are several possible sources for these differences. First, the coupled RegCM-lake model may not represent all of the important processes associated with desiccation. For example, salinity is held uniform throughout the water column, prescribed to the observed value in either 1960 or 1990. However, chemical stratification in the higher salinity, 1990 Aral Sea may inhibit vertical mixing, which would reduce the heat storage in the lake and result in warmer (colder) SSTs in the spring–summer (fall–winter). Second, joining the in situ and satellite datasets could make warming (cooling) appear greater (less) than it really is, as the satellite SSTs are ~0.5°C warmer than the in situ observations. Third, in addition to desiccation, the observed changes may reflect large-scale climatic variability or change. This final factor is addressed in section 6.

b. $P - E$ changes

1) EVAPORATION

The Aral Sea evaporation rate is greater in the Half Lake experiment than in the Full Lake experiment from

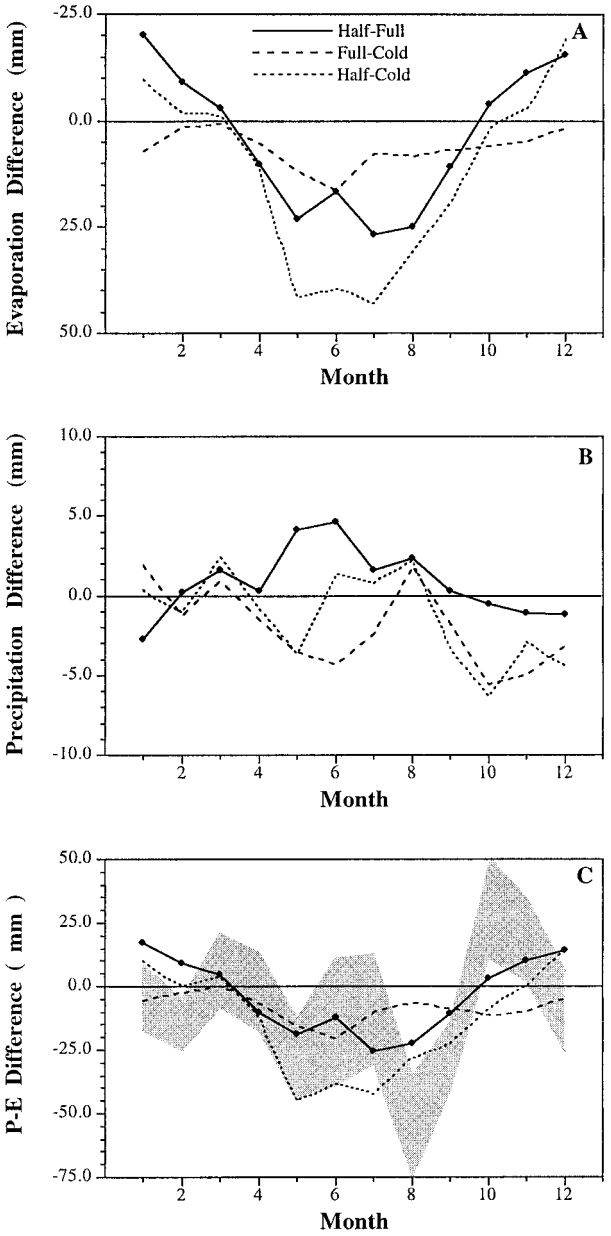

FIG. 15. Simulated monthly averaged changes in (a) evaporation, (b) precipitation, and (c) $P - E$ from desiccation (Half − Full: solid), warming (Full − Cold: dashed), and the combination of desiccation and warming (Half − Cold: dotted). The y axis in the evaporation plot is reversed (negative is up) to match the $P - E$ plot. The observed $P - E$ change (with 95% confidence interval estimates) is shown (gray shaded region). The Half − Full difference is a 5-yr average and the others are 2-yr averages.

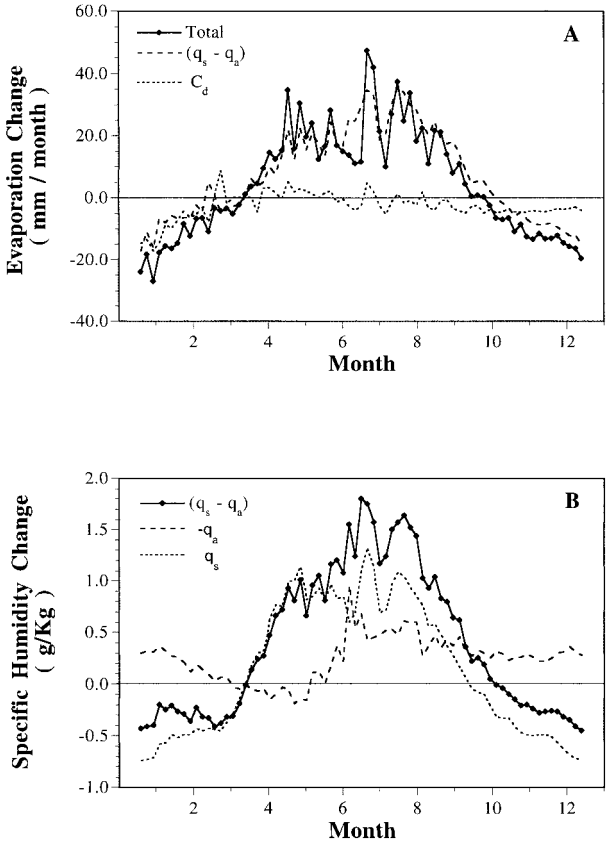

FIG. 16. (a) Simulated changes in Aral Sea evaporation due to desiccation (Half − Full), broken up into the following components: total (solid), $q_s - q_a$ (dashed), and C_d (dotted). (b) Changes (Half − Full) in the surface to air specific humidity difference ($q_s - q_a$) (solid), saturation specific humidity of the surface (q_s) (dotted), and specific humidity of the air ($-q_a$) (dashed). The sign of q_a changes are reversed, so that ''upward'' changes in both q_s and q_a indicate increased evaporation. In both A and B, values are plotted every 5 Julian days, averaged over the 5 yr of the simulations.

April until September, with the greatest change (~15%) in July (Fig. 15a). In contrast, the evaporation rate is lower in the Half Lake experiment between November and February. Overall, the net annual evaporation increases from 1031 to 1081 mm (a 5% change) between the Full and Half Lake experiments (Table 3).

We have separated the evaporation changes into three components, each representing changes in one of the primary hydrometeorologicals variable that influence evaporation [Eq. (3)]: 1) the surface-air difference in specific humidity, $q_s - q_a$; 2) the wind speed over the lake; and 3) the drag coefficient, C_D. Most of the differences in evaporation between the Full and Half Lake experiments are due to changes in $q_s - q_a$, which increases during the spring/summer and decreases during the winter (Fig. 16a). Between October and February, C_D is less in the Half Lake than in the Full Lake experiment (Fig. 16a) because of an increase in near-surface stability (Fig. 6). This reinforces the reduction in evaporation driven by the decrease in $q_s - q_a$. Changes in wind speed between the two simulations are negligible.

The seasonally varying changes in $q_s - q_a$ can be separated into changes in the specific humidity of near-surface air, q_a, and changes in the saturation specific humidity of the surface, q_s. The latter is primarily controlled by surface temperature and only weakly con-

trolled by salinity for the range of salinity examined here. The change in q_s is positive (increased evaporation) from April until August and negative (decreased evaporation) from October until March (Fig. 16b), a result of the simulated changes in SST (Fig. 14). These changes in q_s account for most of the changes in $q_s - q_a$. Therefore, changes in SST are the primary cause of the changes in evaporation resulting from desiccation. Excluding the spring, evaporation in the Half Lake experiment is enhanced by a decrease in q_a. This decrease in q_a is the result of the reduction in lake surface area—replacing half of the Aral Sea with desert reduces regional evaporation, lowering the specific humidity over the extant portion of the lake.

2) PRECIPITATION

The precipitation rate over the Aral Sea is greater in the Half Lake experiment than in the Full Lake experiment between March and September, with a maximum difference of 20% in June (Fig. 15b). Precipitation is slightly less in the Half Lake case between October and January. Overall, the annual precipitation rate is greater in the Half Lake case, but the difference is only 9 mm yr^{-1} or ~5% (Table 3).

The seasonally varying response of precipitation to desiccation is related to the simulated changes in SST—the precipitation rate is greater (reduced) in the Half Lake case when SSTs are warmer (colder) than in the Full Lake case (Fig. 14). During the spring and summer, warmer SSTs in the Half Lake experiment weaken the sea breeze and associated descending air, leading to enhanced precipitation. During autumn and winter, cooler SSTs in the Half Lake case weaken the near-surface gradient of θ_e and convergence over the lake, and therefore lake-effect precipitation.

3) SIMULATED VERSUS OBSERVED $P - E$ CHANGES

Overall, the simulated changes in the annual cycle of $P - E$ resulting from desiccation (Half minus Full Lake) are similar to the observed changes that have accompanied desiccation (Fig. 15c). Both the simulated and observed $P - E$ are more negative between May and September and more positive in October and November. However, the simulated and observed changes differ during the winter—the simulated $P - E$ becomes more positive while the observed $P - E$ is unchanged or becomes more negative.

The simulated change in annual $P - E$ resulting from desiccation is -41 mm (Table 3). This decrease is primarily the result of enhanced evaporation (-50 mm), which is only partially offset by a relatively minor increase in precipitation (9 mm). This result demonstrates that the coupled RegCM-lake model includes a positive feedback to changes in the size of the Aral Sea—a reduction (increase) in surface area and depth results in more negative (positive) $P - E$ over the lake. However, the simulated change in annual $P - E$ resulting from desiccation is only ~30% of the observed change that has accompanied desiccation, with most of the difference arising during August and September (Figs. 3c and 15). If the model adequately represents the processes associated with desiccation and if the observed data are accurate, then the difference between the simulated and observed changes in $P - E$ indicates that processes other than desiccation must have contributed to the observed hydrologic changes.

6. Influence of climatic variability or change

In this section, we examine how large-scale climatic variability or change has influenced the water balance of the Aral sea between 1960 and the mid-1990s. This is accomplished by comparing the Full Lake and Cold experiments over their common 2-yr interval (Table 2). The only difference between these two simulations is the perturbation (1.5°C cooling with constant relative humidity) of the meteorological boundary conditions in the Cold case. We compare these two simulations as ''Cold minus Full Lake'' to examine the effects of the perturbation. However, we reverse these differences (Full Lake minus Cold) in our comparison with the observed changes, so that the simulated difference between the two experiments can be equated to the progressive warming observed in central Asia between 1960 and the mid-1990s.

a. Air and sea surface temperatures

In comparison with the Full Lake experiment, 2-m air temperatures in the Cold experiment are typically 1.5°C cooler throughout the domain, which is equal to the perturbation of the boundary conditions. This shows that the perturbation applied at the lateral boundaries of the domain influences the entire domain, including the Aral Sea. However, departures from a 1.5°C decrease do exist. During summer, the change in air temperature is less than the perturbation in areas that have abundant soil moisture or open surface water, including the Aral Sea (Fig. 17a). A negative feedback to the prescribed cooling exists in these relatively wet areas—the temperature decrease leads to reduced evaporation, a higher Bowen ratio, and therefore a relatively higher surface temperature. During winter, the temperature change is less than the perturbation to the south and east of the Aral Sea (Fig. 17b), again demonstrating the effects of feedbacks within the domain.

Evaporation from the Aral Sea is ''unlimited.'' Therefore, the negative feedback resulting from the dependence of evaporation on temperature limits the cooling of Aral SSTs at times when the latent heat flux is an important component of the SEB. For example, the decrease in Aral SSTs between April and December is ~1.0°C (Fig. 14). An increase in ice cover is responsible

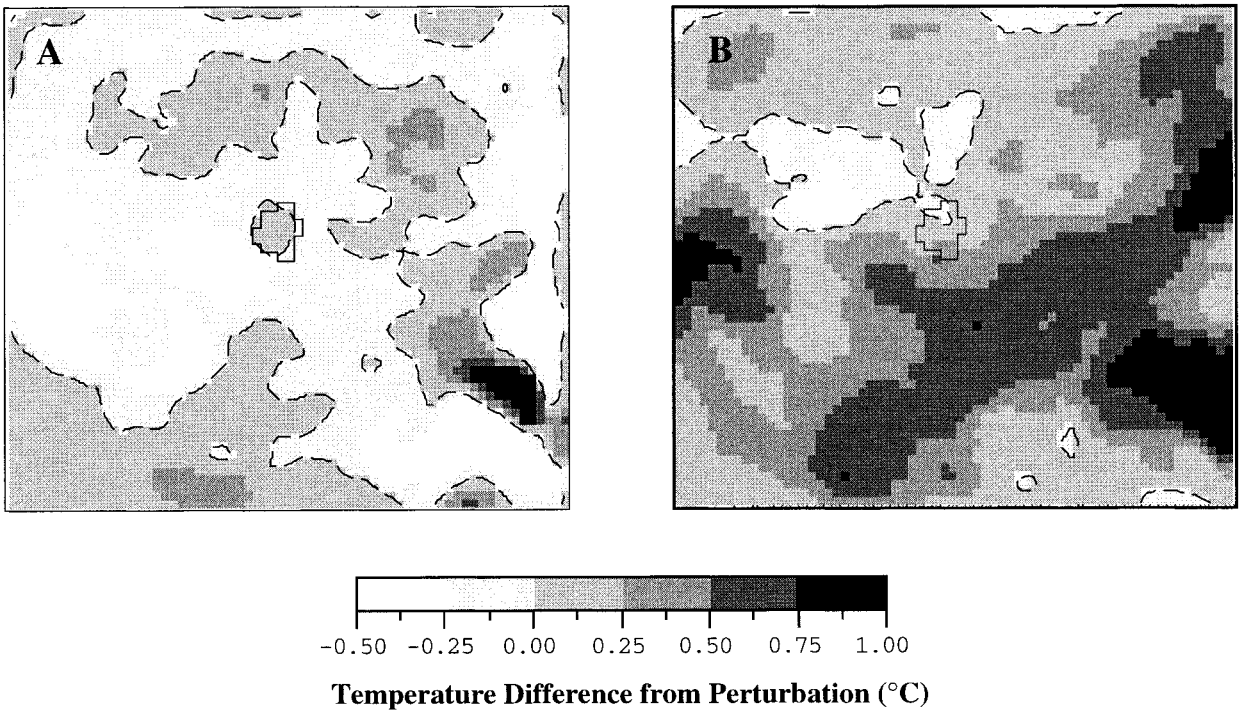

FIG. 17. Departure from a 1.5°C cooling in the Cold experiment, relative to the Full Lake experiment, for (a) summer and (b) winter averaged over the two simulated years. Areas in which the departure is positive have a change less than −1.5°C, and vice versa.

for the cooling in January that is greater than the perturbation.

Based on the differences between the Full and Cold experiments, we conclude that the effect of climatic variability or warming between 1960 and the mid-1990s would be to increase SSTs by an amount slightly less than air temperature changes between spring and autumn, and perhaps more during winter. The simulated changes in SST due to warming alone (Full Lake minus Cold) are not consistent with the observed SST changes (Fig. 14). Simulated SSTs increase by ~1°C during the spring through autumn and by a greater amount during the winter. The observed SST changes are several times more positive in the spring and early summer. In addition, the observed changes are negative in the autumn and winter, which is the opposite of the simulated change.

b. Precipitation

Differences in precipitation between the Cold and Full Lake experiments are not spatially homogenous. During summer, precipitation in the Cold experiment decreases in the northern half of the domain and to the east of the Aral (Fig. 18a). The large percentage increases in the southern, arid portion of the domain represent only small changes in absolute magnitude. During winter, precipitation in the Cold experiment is typically less (by <10%) than in the Full Lake case (Fig. 18b). In contrast, precipitation increases over the Aral Sea and in the surrounding areas.

Between May and December, precipitation over the Aral Sea is greater in the Cold than in the Full Lake experiment, with the greatest changes occurring in May–June and October–November (20%–25%). Part of this increase is related to enhanced precipitation across a broad region (Fig. 18). Precipitation is also locally enhanced over the Aral Sea. During the summer, the negative temperature–evaporation feedback described above reduces the lake–land thermal contrast, which enhances warm-season precipitation. During the fall and early winter, the lake–land thermal contrast is enhanced because the lake surface cools less than the surrounding land. This increases lake-effect precipitation. These results suggest that precipitation should decrease through time as air temperature increases (i.e., Full Lake minus Cold), with a net annual change of −25 mm (Fig. 15b and Table 4).

c. Aral Sea water balance

1) EVAPORATION

In comparison with the Full Lake experiment, evaporation from the Aral Sea is reduced throughout the year in the Cold experiment. This suggests that the observed warming between 1960 and the mid-1990s would yield an increase in evaporation through time (Full Lake mi-

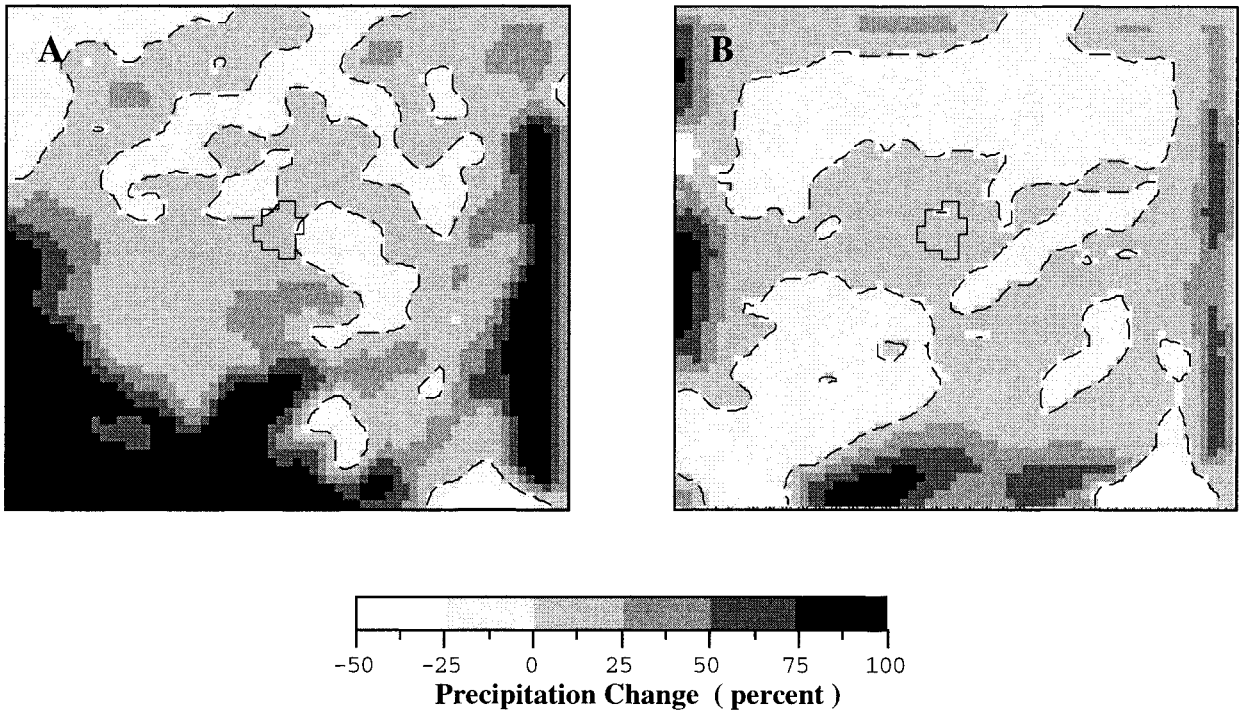

FIG. 18. Percent precipitation change (Cold − Full) during (a) summer and (b) winter averaged over the two simulated years.

nus Cold) (Fig. 15a). The greatest change in the Cold experiment occurs in May and June when the evaporation rate decreases by more than 10 mm month^{-1}. The net annual decrease in evaporation is 78 mm or ~8% (Table 4).

The reduced evaporation in the Cold experiment is primarily the result of a decrease in the surface-to-air specific humidity gradient, $q_s - q_a$. In the Cold experiment, both q_s and q_a decrease in all months—the former because SSTs are lower and the latter because air temperature is lower and relative humidity is nearly unchanged. However, the reduction in q_s is always greater in magnitude than that of q_a. The change in specific humidity (q_s or q_a) resulting from a decrease in temperature is a nonlinear function of temperature and is also scaled by the relative humidity. Whereas the relative humidity at the lake surface is 100%, the relative humidity of the overlying air (~40 m) is between 50% and 90%, depending on the season. Therefore, even though Aral SSTs cool slightly less than the overlying air, the decrease in q_s is always greater than the decrease in q_a. The resulting decrease in $q_s - q_a$, and hence in evaporation, is greatest during the summer because 1) saturation vapor pressure has greater temperature sensitivity at higher temperatures and 2) the relative humidity of the air is lowest during this season, allowing for the greatest difference between the changes in q_s and q_a. The simulated change in evaporation is primarily the result of the shape of the saturation vapor pressure curve and the difference in relative humidity between the lake surface and the overlying air. Therefore, we feel confident that the simulated response to the prescribed temperature change is valid, even given the simple perturbation.

TABLE 4. Simulated water balance of the Aral Sea in the Full Lake and Cold experiments and the differences between them (Full − Cold). All units: mm yr^{-1}. The observed change in $P - E$ between 1960 and 1992 is also shown.

	Precipitation	Evaporation	$P - E$
Model: Full	232	1039	−806
Model: Cold	257	961	−704
Simulated change: Full − Cold	−25	78	−102
Observed change			−141

2) $P - E$

In comparison with the Full Lake experiment, $P - E$ is more positive in all months in the Cold experiment because precipitation is higher and evaporation is lower. This change is equivalent to $P - E$ becoming more negative through time (Fig. 15c and Table 4) as air temperatures have increased between 1960 and the mid-1990s. The simulated net annual decrease in $P - E$ due to warming (i.e., Full minus Cold) is 102 mm, which is similar to the observed decrease of 141 mm. However, the simulated $P - E$ changes are slightly negative (~−10 mm) in all months whereas the observed changes are much more negative during August and Septem-

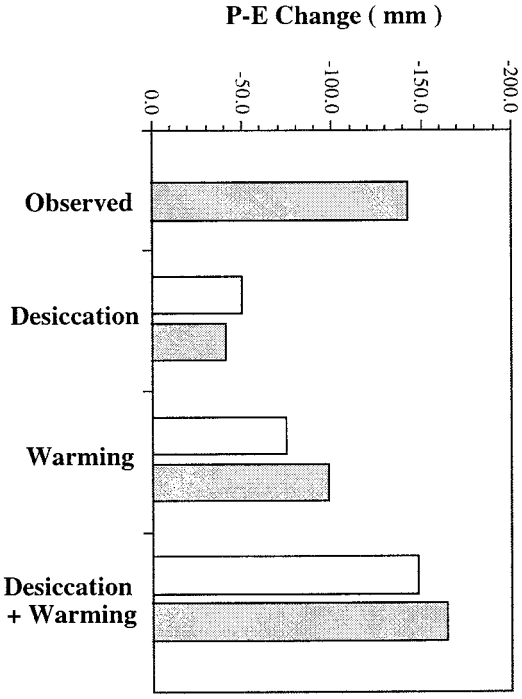

FIG. 19. Observed net annual $P - E$ change and the simulated net annual evaporation (white) and $P - E$ (gray) changes from desiccation (Half − Full), warming (Full − Cold), and the combination of desiccation and warming (Half − Cold).

ber and are positive in October and November (Fig. 15c).

7. Summary

The simulated SST changes resulting from desiccation are similar to those that have been observed between 1960 and the mid-1990s—both simulated and observed SSTs have increased during spring and summer and have decreased during the autumn and winter (Fig. 14). However, the simulated warming is less than observed by several degrees in the late spring and early summer. The simulated changes in the annual cycle of $P - E$ resulting from desiccation are also similar to observed changes (Fig. 15c). However, the simulated decrease in $P - E$ is not as large as observed during the summer and is positive in the winter when no change is apparent in the observed record. The result is that the simulated net annual change in $P - E$ is −40 mm, which is only ~30% of the observed decrease of −141 mm (Fig. 19). These results suggest that desiccation is an important source of the hydrologic changes that have occurred between 1960 and the mid-1990s, but other processes must also be important.

Air temperature has increased substantially across all of central Asia throughout the desiccation interval, which may be the result of enhanced greenhouse gas concentrations or natural climatic variability. The simulated effects of ''warming'' on the hydrologic conditions of the Aral Sea do not closely match the observed changes. Even though the simulated decrease in net annual $P - E$ is similar to the observed decrease (Fig. 19), the simulated changes in SST and $P - E$ differ substantially from the observed changes at the monthly timescale (Figs. 14 and 15). The simulated SST changes are positive and the $P - E$ changes are negative in all months. In contrast, observations indicate that the sign of both SST and $P - E$ changes varies throughout the year.

TABLE 5. Simulated water balance of the Aral Sea in the Half Lake and Cold experiments and the differences between them (Half − Cold). All units: mm yr^{-1}. The observed change in $P - E$ between 1960 and 1992 is also shown.

	Precipitation	Evaporation	$P - E$
Model: Full	241	1113	−872
Model: Cold	257	961	−704
Simulated change: Full − Cold	−16	152	−168
Observed change			−141

The simulated hydrologic response to the combined effects of desiccation and warming, as represented by the difference between the Half Lake and Cold experiments (Table 2), matches the observed SST and $P - E$ changes more closely than the response to each forcing alone (Figs. 15 and 19, Table 5). The simulated and observed $P - E$ changes are similar on the monthly (Fig. 15) and annual timescales (Fig. 19). In addition, the simulated SST changes closely resemble the observed changes (Fig. 14), except that the simulated change is too positive between August and October.

Between 1960 and the mid-1990s, anthropogenic reduction of river inflow to the Aral Sea resulted in a >50% decrease of surface area and mean lake depth. We present the following scenario as an explanation for the observed changes in $P - E$ and SST that have accompanied desiccation, based on a series of coupled regional climate-lake model experiments.

SSTs warmed in the spring and summer and cooled in autumn and winter in response to the decrease in lake depth and the associated reduction in seasonal heat storage within the water column. These SST changes resulted in increased evaporation during the spring and summer and reduced evaporation during autumn and winter. The humidity over the lake has decreased because of the reduction in Aral Sea surface area. This enhances evaporation in all seasons. Overall, desiccation yields an increase in annual evaporation of 50 mm because the increase in evaporation rate during the warm season more than offsets the decrease in evaporation rate in the cold season. Desiccation enhances the precipitation rate over the lake surface (~10 mm yr^{-1}). This increase only partially offsets the enhanced evaporation because precipitation is a minor component of the Aral Sea hydrologic budget. The net effect of desiccation is to decrease $P - E$ over the Aral Sea by ~40

mm yr^{-1} (Fig. 19), which indicates a positive feedback exists that enhances changes in lake size.

The primary effect of desiccation on the hydrologic conditions of the Aral Sea is to alter the annual cycle of SST and $P - E$. In contrast, large-scale warming that has accompanied desiccation has influenced Aral Sea hydrologic conditions most strongly on the annual timescale. SSTs have increased throughout the year in response to the observed warming, enhancing evaporation in all seasons. Warming has resulted in a reduction of on-lake precipitation, but again the impact on the hydrologic budget is not substantial. The net effect of warming is to decrease $P - E$ over the lake by ~100 mm yr^{-1}, a change of ~12%. Therefore, we hypothesize that warming is the primary source for the observed decrease in annual $P - E$ over the Aral Sea.

This model-based scenario is consistent with the observed changes in air temperature from the Aral Sea region (Small et al. 2001). Near the Aral Sea, desiccation has resulted in warmer air temperatures during spring and summer, cooler air temperatures during autumn and winter, and an increase in diurnal temperature range throughout the year. In contrast, large-scale climatic variability or change has resulted in warmer air temperature in all seasons, except perhaps in spring. Together, these results demonstrate that it is critical to separate regional and large-scale climatic and hydrologic changes when assessing the response of the climate system to land surface modifications.

Acknowledgments. This research was supported by NSF ATM-9632304. We thank C. Shields, A. Ewing, B. Gustav, and C. Morrill for their assistance. Two anonymous reviewers provided helpful comments.

REFERENCES

Anthes, R. A., E. Y. Hsie, and Y. H. Kuo, 1987: Description of the Penn State/NCAR Mesoscale Model Version 4 (MM4). NCAR Tech. Note NCAR/TN-282, 66 pp.

Atkinson, B. W., 1981: *Meso-Scale Atmospheric Circulations.* Academic Press, 495 pp.

Bates, G. T., S. W. Hostetler, and F. Giorgi, 1995: Two-year simulation of the Great Lakes Region with a coupled modeling system. *Mon. Wea. Rev.,* **123,** 1505–1522.

Bortnik, B. H., 1990: *Hydrometeorology and Hydrology of the Seas of the Soviet Union: The Aral Sea* (In Russian). Hydro-meteorological Publisher, 412 pp.

Briegleb, B. P., 1992: Delta-Eddington approximation for solar radiation in the NCAR Community Climate Model. *J. Geophys. Res.*, **97** (D7), 7603–7612.

Changnon, S. A., and D. M. A. Jones, 1972: Review of the influences of the Great Lakes on weather. *Water Resour. Res.*, **8,** 360–371.

Dickinson, D. R., J. H. Yepsen, and J. V. Hales, 1965: Saturated vapor pressures over Great Salt Lake brines. *J. Geophys. Res.,* **70** (2), 500–503.

Dickinson, R. E., A. Henderson-Sellers, and P. J. Kennedy, 1993: Biosphere–Atmosphere Transfer Scheme (BATS) version 1e as coupled to the NCAR Community Climate Model. NCAR Tech. Note NCAR/TN-387 + STR, 72 pp.

Eichenlaub, V. L., 1970: Lake effect snowfall to the lee of the Great Lakes: Its role in Michigan. *Bull. Amer. Meteor. Soc.,* **51,** 403–412.

Ellis, A. W., and D. J. Leathers, 1996: A synoptic climatological approach to the analysis of lake-effect snowfall: Potential forecasting applications. *Wea. Forecasting,* **11,** 216–229.

Gill, A. E., 1982: *Atmosphere–Ocean Dynamics.* Academic Press, 662 pp.

Giorgi, F., and C. Shields, 1999: Tests of precipitation parameterizations available in the latest version of the NCAR regional climate model (RegCM) over continental United States. *J. Geophys. Res.,* **104,** 6353–6375.

——, M. R. Marinucci, and G. T. Bates, 1993a: Development of a second-generation regional climate model (RegCM2). Part I: Boundary-layer and radiative transfer processes. *Mon. Wea. Rev.,* **121,** 2794–2813.

——, ——, and ——, 1993b: Development of a second-generation regional climate model (RegCM2). Part II: Convective processes and assimilation of lateral boundary conditions. *Mon. Wea. Rev.,* **121,** 2814–2832.

Graham, J., 1966: Secchi disc observations and extinction coefficients in the central and eastern North Pacific Ocean. *Limnol. Oceanogr.,* **11,** 184–190.

Grell, G. A., 1993: Prognostic evaluation of assumptions used by cumulus parameterizations. *Mon. Wea. Rev.,* **121,** 764–787.

Henderson-Sellers, B., 1985: New formulation of eddy diffusion thermocline models. *Appl. Math. Model.,* **9,** 441–446.

——, 1986: Calculating the surface energy balance for lake and reservoir modeling: A review. *Rev. Geophys.*, **24,** 625–649.

Hjelmfelt, M. R., 1990: Numerical study of the influence of environmental conditions on lake-effect snowstorms over Lake Michigan. *Mon. Wea. Rev.,* **118,** 138–150.

——, 1992: Orographic effects in simulated lake-effect snowstorms over Lake Michigan. *Mon. Wea. Rev.,* **120,** 373–377.

Holtslag, A. A. M., E. I. F. de Bruin, and H. L. Pan, 1990: A high resolution air mass transformation model for short-range weather forecasting. *Mon. Wea. Rev.,* **118,** 1561–1575.

Hostetler, S. W., and P. J. Bartlein, 1990: Simulation of lake evaporation with application to modeling lake level variations of Harney–Malheur Lake, Oregon. *Water Resour. Res.,* **26,** 2603–2612.

——, F. Giorgi, G. T. Bates, and P. J. Bartlein, 1994: Lake–atmosphere feedbacks associated with Paleolakes Bonneville and Lahontan. *Science,* **263,** 665–668.

Houghton, J. T., L. G. Meira Filho, B. A. Callander, N. Harris, A. Kattenberg, and K. Maskell, Eds., 1996: *Climate Change 1995: The Science of Climate Change.* Cambridge University Press, 572 pp.

Hsu, H.-M., 1987: Mesoscale lake-effect snowstorms in the vicinity of Lake Michigan: Linear theory and numerical simulations. *J. Atmos. Sci.,* **44,** 1019–1021.

Hurrell, J. W., and H. Van Loon, 1997: Decadal variations in climate associated with the North Atlantic oscillation. *Climatic Change,* **36,** 301–326.

Kiehl, J. T., and B. P. Briegleb, 1993: The relative roles of sulfate aerosols and greenhouse gases in climate forcing. *Science,* **260,** 311–314.

Legates, D. R., and C. J. Willmott, 1990: Mean seasonal and spatial variability in gauge-corrected, global precipitation. *Int. J. Climatol.,* **10,** 111–127.

Lofgren, B. M., 1997: Simulated effects of idealized Laurentian Great Lakes on regional and large-scale climate. *J. Climate,* **10,** 2847–2858.

McClain, E. P., 1989: Global sea surface temperatures and cloud clearing for aerosol optical depth estimates. *Int. J. Remote Sens.,* **10,** 767–769.

——, W. G. Pichel, and C. C. Walton, 1985: Comparative performance of AVHRR-based multichannel sea surface temperatures. *J. Geophys. Res.,* **90,** 11 587–11 601.

Micklin, P. P., 1988: Desiccation of the Aral Sea: A water management disaster in the Soviet Union. *Science,* **241,** 1170–1176.

Miner, T. J., and J. M. Fritsch, 1997: Lake-effect rain events. *Mon. Wea. Rev.*, **125,** 3231–3248.

Morton, F. I., 1967: Evaporation from large deep lakes. *Water Resour. Res.*, **3,** 181–200.

Niziol, T. A., W. R. Snyder, and J. S. Waldstreicher, 1995: Winter weather forecasting throughout the eastern United States. Part IV: Lake effect snow. *Wea. Forecasting*, **10,** 61–77.

Patterson, J. C., and P. F. Hamblin, 1988: Thermal simulation of a lake with winter ice cover. *Limnol. Oceanogr.*, **33,** 323–338.

Pielke, R. A., 1984: *Mesoscale Meteorological Modeling.* Academic Press, 612 pp.

Sadov, A. V., and V. V. Krasnikov, 1987: Detection of foci of subaqueous subsurface water discharge into Aral Sea by remote sensing methods. *Problemy Osvoeniya Pustyn*, **1,** 28–36.

Schar, C., C. Frei, D. Luthi, and H. C. Davies, 1996: Surrogate climate-change scenarios for regional climate models. *Geophys. Res. Lett.*, **23,** 669–672.

Small, E. E., F. Giorgi, and L. C. Sloan, 1999a: Regional climate model simulation of precipitation in central Asia: Mean and interannual variability. *J. Geophys. Res.*, **104,** 6563–6582.

——, L. C. Sloan, F. Giorgi, and S. Hostetler, 1999b: Simulating the water balance of the Aral Sea with a coupled regional climate-lake model. *J. Geophys. Res.*, **104,** 6583–6602.

——, ——, and D. Nychka, 2001: Changes in surface air temperature caused by desiccation of the Aral Sea. *J. Climate*, **14,** 284–299.

Trenberth, K. E., 1992: Global analyses from ECMWF and atlas of 1000 to 10 mb circulation statistics. NCAR Tech. Note NCAR/TN-373 + STR, 191 pp.